NONLINEAR ANALYSIS OF ACOUSTIC DUAL HELMHOLTZ RESONATORS

BY

MAHER OMAR AL TURK

A Thesis Presented to the

DEANSHIP OF GRADUATE STUDIES

KING FAHD UNIVERSITY OF PETROLEUM & MINERALS

DHAHRAN, SAUDI ARABIA

In Partial Fulfillment of the
Requirements for the Degree of

MASTER OF SCIENCE

In

MECHANICAL ENGINEERING

December 2018

KING FAHD UNIVERSITY OF PETROLEUM & MINERALS

DHAHRAN- 31261, SAUDI ARABIA

DEANSHIP OF GRADUATE STUDIES

This thesis, written by MAHER AL TURK under the direction his thesis advisor and approved by his thesis committee, has been presented and accepted by the Dean of Graduate Studies, in partial fulfillment of the requirements for the degree of **MASTER OF SCIENCE IN MECHANICAL ENGINEERING**

Thesis Committee

Thesis Advisor

Dr. Muhammad Hawwa

Department Chairman

Dr. Zuhair Mattoug Gasem

Committee Member

Dr. Yehia Khulief

Dean of Graduate Studies

Dr. Salam A. Zummo

Committee Member

Dr. Fadi Al-Badour

26/2/19

Date

In the name of Allah, the Most Gracious and the Most Merciful

Dedicated

to

My Beloved Parents, Brothers, and Friends

ACKNOWLEDGMENTS

All praise and thanks are due to Almighty Allah, Most Gracious and Most Merciful, for his immense beneficence and blessings. He bestowed upon me health, knowledge, and patience to complete this work. May peace and blessings be upon Prophet Muhammad (PBUH), his family and his companions.

Thereafter, acknowledgment is due to KFUPM for the support extended towards my research through its remarkable facilities and for granting me the opportunity to pursue graduate studies.

I acknowledge, with sincere gratitude and appreciation, the inspiration, encouragement, valuable time and continuous guidance given to me by my dissertation advisor, Dr. Muhammad Hawwa. I am profoundly grateful to my committee members Dr. Yehia Khulief, Dr. Fadi Al-Badour for their valuable guidance and support.

My heartfelt thanks are due to my parents and brothers for their prayers, guidance, and moral support throughout my academic life. My parents' advice, to strive for excellence has made all this work possible. Special thanks are due to my senior colleagues at the university, for their help, prayers and who provided wonderful company and good memories that will last a lifetime.

TABLE OF CONTENTS

LIST OF TABLES

LIST OF FIGURES

LIST OF ABBREVIATIONS

CFD	Computational fluid dynamics
DOF	Degree of Freedom
HVAC	Heating, Ventilation and Air Conditioning
HHR	Helmholtz Resonator
HR	Helmholtz Resonator
FR	Frequency Ratio
IR	Insertion Loss
NNM	Nonlinear normal Mode
NR	Noise Reduction
SPL	Sound Pressure Level
TL	Transmission Loss
TMD	Tuned Mass Damper

NOMENCLATURE

A_c	The effective area of the HHR Neck
A_p	The effective area of the Duct
A_v	Area of the HHR Cavity
c_0	Speed of Sound
c_1, c_2	Dimensionless Linear Damping Coefficient
c_3, c_4	Dimensionless Nonlinear Damping Coefficient
c_t	Kundt Tube Damping Coefficient
f	Natural Frequency
K	Stiffness Matrix
k_1	Quadratic Nonlinear Stiffness Coefficient
k_2	Cubic Nonlinear Stiffness Coefficient
k_t	Kundt Tube Stiffness Coefficient
k	Wave Number
L_e	Effective Length of the HHR Neck
L_c	Length of the HHR Neck
L_c'	Effective Length of the HHR Neck
L_v	Length of the HHR Cavity
m	Equivalent Mass of the fluid in the HHR Neck or Kundt Tube
M	Effective Mass of the Fluid in the Cavity

p	Pressure
P	Pressure Amplitude
p_0	Atmospheric Pressure
R	Damping Matrix
R_c	Radius of the Neck
r_1	Mass Ratio
r_2	Frequency ratio
S	The effective area of the HHR Neck or Kundt Tube
t	Time
t*	Dimensionless Time
T_1	The amplitude of the Incident Sound Pressure Wave
T_2	The amplitude of the Transmitted Sound Pressure Wave
V	The volume of the HR Cavity or Coupling Box
ω_0	Natural Frequency
x_c	Displacement of the HR
x	Dimensionless Displacement of the HR
x_t	Kundt Tube Displacement
Z_{vis}	Impedance of the Acoustic Friction
$Z_{H,in}$	Acoustic Impedance
ρ_1, ρ_0	Density
$\emptyset$	Potential Function

δ	Linear damping coefficient
ζ	Coefficient of the total Hydraulic Resistance
Ω	Frequency Ratio

THESIS ABSTRACT (ENGLISH)

FULL NAME : MAHER OMAR MOHAMMAD AL TURK

THESIS TITLE : NONLINEAR ANALYSIS OF ACOUSTIC DUAL HELMHOLTZ RESONATORS

MAJOR FIELD : MECHANICAL ENGINEERING

DATE : DEC 2018

Helmholtz resonators are often used to reduce noise in different applications such as HVAC systems. This study focuses on the effectiveness of dual HHRs in reducing noise. Methods for enhancing their performance are realized by applying nonlinear analysis for different configurations of HHRs to accommodate the excess average pressure inside the resonator, which results from a hydrodynamic origin, due to vortex shedding at the outflow from neck opening. Dual HHRs provide a necessary solution for attenuating the noise at two distinct frequencies, which is needed when using ducted rotating machineries with varying loads. Attention is also given to the effect of the geometry of the HHR on its resonant frequency and its noise attenuation capability, which shows that when the area ratio of the two necks is increased, the ratio of resonant frequencies increased. Nonlinear HHRs show a softening behavior at low sound pressure levels and hardening behavior at high sound pressure levels. The possibility of energy transfer from one acoustical mode to the dual nonlinear HHR through a Kundt tube and a coupling box has been investigated.

MASTER OF SCIENCE DEGREE

KING FAHD UNIVERSITY OF PETROLEUM AND MINERALS

Dhahran, Saudi Arabia

THESIS ABSTRACT (ARABIC)

ملخص الرسالة

الاسم: ماهر عمر محمد الترك

عنوان الرسالة: دراسة فعالية الحجيرات التوسعية المزدوجة من خلال تطبيق التحليل اللاخطي

التخصص:الهندسة الميكانيكية

تاريخ التخرج: 1440 هـ - (ديسمبر 2018 م)

حجيرات التوسع تستخدم غالبا للحد من الضوضاء الصوتية في الأنظمة المختلفة كأنظمة التكييف المركزي. تركز هذه الدراسة على فعالية حجيرات التوسع المزدوجة في الحد من الضوضاء في داخل مسارات الهواء. طرق تحسين أداء رنانات هلمهولتز تمت من خلال تطبيق التحليل اللاخطي للتكوينات المختلفة لرنانات هيلمهولتز لتفسير متوسط الضغط الزائد داخل الرنان ، والذي ينتج من أصل هيدروديناميكي ، عند خروج دوامات المائع من فوهة الرنان. بينت نتائج هذه الرسالة أن الرنانات المزدوجة تعتبر حلاً ضروريًا للتخفيف من الضوضاء عند وجود ترددين مختلفين، والتي تحدث غالبا عند استخدام أجهزة التكييف ذات التردد المتغير. تمت دراسة تأثير أبعاد الهيلمهولتز ريزونيترعلى ترددها الرنيني وقدرتها على تخفيف الضوضاء والتي بينت أنه عند زيادة نسبة المساحة للعنق الأول بالنسبة إلى الثاني فإن ذلك يقود إلى زيادة في النسبة بين الترددين الأول والثاني أيضا. كما و أظهر السلوك غير الخطي لرنان الهيلمهولتز أن التردد الرنيني يتناقص مع زيادة مستويات الصوت المنخفضة بينما يتحول هذا السلوك عند مستويات الصوت المرتفعة ليصبح زيادة بالتردد الرنيني مع الزيادة بمستوى الصوت. وتمت دراسة نظام فريد لنقل الطاقة المستهدفة باستخدام الكوندت تيوب و صندوق الاقتران إلى رنان هيلمهولتز المزدوج عبر تطبيق السلوك غير الخطي.

شهادة ماجستير علوم

جامعة الملك فهد للترول والمعادن

الظهران- المملكة العربية السعودية

CHAPTER 1

INTRODUCTION

1.1 Background

In giving a brief description of the background of acoustics, it is considered as both a classical and a modern field because it has been studied for centuries. Its origins begin with the study of the mechanical vibrations and the transmission/propagation of these waves through mechanical vibrations and, as we can see, it is still under intensive research to this date. Not only that but studies and analysis have been conducted into the various aspects of the distinctive characteristics of the fundamental physical processes which are occurring or taking place in sound and other types of waves, along with the practical effect and implications of these waves in modern life. The study of sound waves also leads to physical principles that can be applied to the study of all waves.

From a definition point of view, any branch of science which deals with the magnitude of waves (amplitude), repeated cycles per second (frequency), the traveling of waves (transmission/propagation), and their formation complexity is considered to be an acoustical science.

The branch of acoustics has wide-ranging applications which are core to human comfort and the technological index. From many existing types, the main applications of acoustic technology include music, the study of geologic, atmospheric and underwater phenomena, medical processing and structural defects analysis [1].

Sound levels and their reception by the human ear are based on perception and the frequency, periodicity, and amplitude of the sound. Let us take the example of music where it is clear that it is pleasant to the ear because of its periodicity and controlled repeatability. On the other hand, annoying and disturbing sounds are often described as noise. Often when we compare the waveforms for both types using a visual representation of sound, music has more patterns and more rhythmic periodicity, whereas noise is jagged and sporadic. In HVAC the air whishing sound in ducts is not acceptable, even though it is also constant in amplitude and frequency. Similarly, in machines, motors, etc.… we have high sounds with the same amplitude which are disturbing to the human ear because of their amplitude. Consequently, any auditory noise perceived by the human ear as annoying is considered to be noise, even though it is periodic or rhythmic [2].

Sound levels are commonly measured in decibels (dB), which is a logarithmic way of describing a ratio of either sound power or sound pressure levels. The human ear can detect a wide range of sound pressure levels. Sounds can be very soft, such as the ticking of a wristwatch, or very loud, such as a top fuel dragster doing a burnout [23]. Figure 1.1 shows different sources of sounds pressure levels based on the activity. It is noticed that 115 dB is equivalent to the sound of a baby crying. This level of noise is located below the human pain threshold and may lead to irreparable and permanent damage, especially with frequent, consistent exposure over a long time.

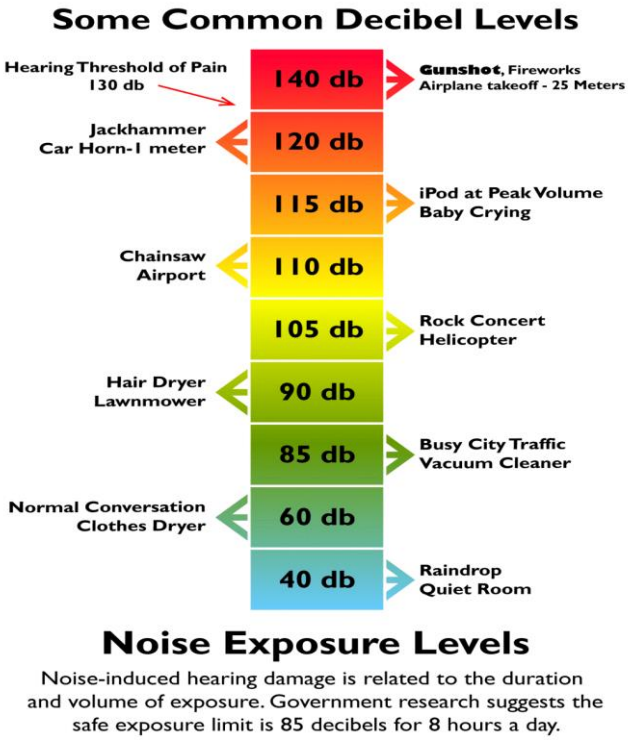

Figure 1.1: Noise Exposure Levels [21]

Sound loudness, which is measured in (phon), depends on the sound pressure level, as well as the frequency at which the sound is occurring. Figure 1.2 shows that 100 phon of loudness is sensed by the human ear. However, its sound pressure level varies across the frequency range; which is because of the human ear's sensitivity at the different frequencies.

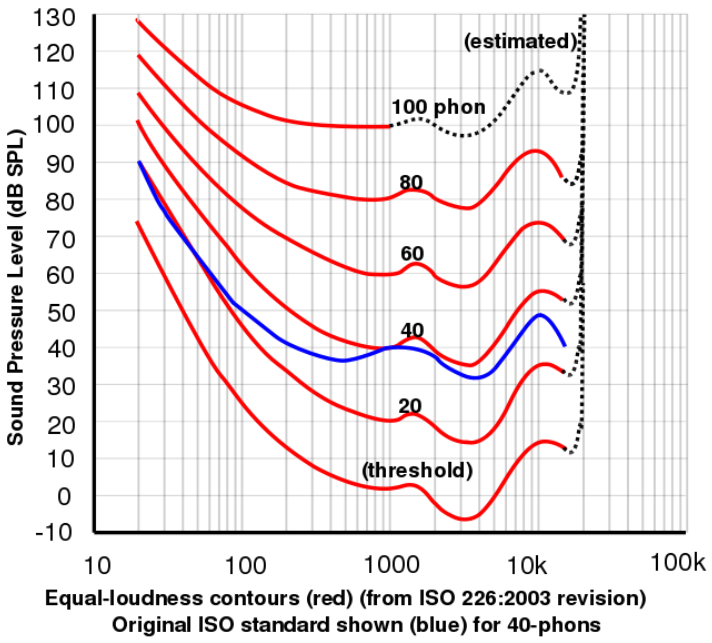

Figure 1.2: Equal Loudness Contours [21]

Many sound attenuators have been developed ranging from the addition of secondary attachment-based Helmholtz resonators to the embedding type which includes lining structures having porous or other materials [3].

In the following section, different types of acoustic attenuators are discussed and classified depending on their configuration.

1.2 Acoustic Attenuators

Acoustic attenuators are used in sound suppressions, and they are applicable when we have the requirement to reduce the noise generated by air or gas flow, and the purpose is to reduce the sound without affecting the air or gas flow itself, and not only that but also maintaining the pressure drop as low as possible. Also, they have wide-ranging

applications including a variety of domestic types, industrial types, automobile based and mixed applications.

The main application of these attenuators is in the fan inlets systems, HVAC systems, radiator discharge, cooling towers, plant dryers, compressor systems, turbines, etc., so in short, any field which has the air flow to and from the generating or consuming equipment which is generating noise. The purpose of acoustic attenuators is to reduce the noise to an acceptable industry level [4].

1.2.1 Types of Acoustic Attenuators

Several basic types of acoustic attenuators are available, based on their design or construction, which, in its turn, is dictated by the peculiarities of a specific application.

1) Absorptive or Dissipative Attenuators

Absorptive attenuators are based on the material used for the attenuation purpose. That is why the thickness parameters are selected depending on the frequency requirement. In the working of these materials, some of the sound power incidents on it are also converted into heat — silencers to attenuate the sound waves (noise) depending on a material used to absorb the sound waves. Absorptive attenuators have found their applications mostly in HVAC systems as shown in figure 1.3. It also comes in the example of passive type attenuators [5].

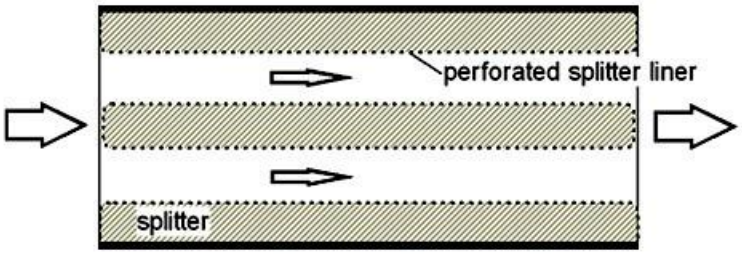

Figure 1.3: Absorptive Attenuator [24]

2) Reactive or Reflective Attenuators

The reflective or reactive type of attenuators shown in figure 1.4 use the mechanism of reflection, anti-resonance, and destructive interference (noise canceling) to achieve high-frequency attenuation as per selection. The reflection provides the extended flow paths, providing us with an interference effect suppressing the noise. Not only that, the cavities and membranes can be tuned to obtain the attenuation at low frequencies. The reactive attenuators are more efficient in the low-frequency range, and the most common example including the reactive attenuators is an expansion chamber and the applications which are feasible for the ones producing pure tones, e.g. fixed speed machinery [5].

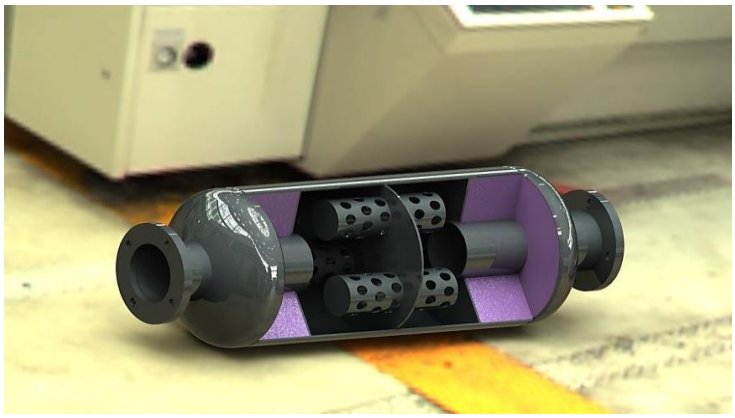

Figure 1.4: Reflective or Reactive Attenuator [25]

3) Active Attenuators

Active attenuators use sensors, microphones and anti-noise generator speakers to suppress the sound sources as shown in figure 1.5. The typical form is that a control system driven by sensors and precise microphones generates the mirror-image of the sound wave offering destructive interference, a result which produces a zero net sound effect. The active attenuators are the advanced type of attenuators, and their design requires high precision as a slight change in the position of a sound generating speaker can result in constructive interference providing the opposite effect. The active type of attenuators are efficient for steady noise field applications and they include fans, engines, and similar machinery. On the opposite side, they are not suitable for broadband noise reduction [6].

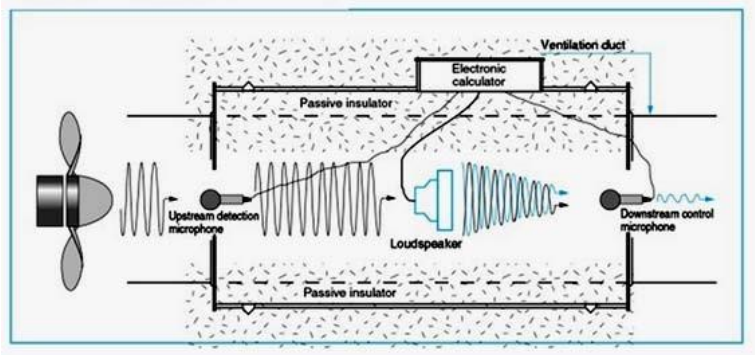

Figure 1.5: Active Attenuator [24]

4) Helmholtz Resonators

The design of Helmholtz has always been based on one common configuration which includes a neck cavity. In more detail the resonator is always made of a cavity which communicates with the main duct body through the neck structure. The fabrication type is

general for all of the Helmholtz resonators with changes in the design, dimensions, and installation configuration. These resonators have proved their worth on the narrow band of the low-frequency noise. CAI and Cheuk [7] used one of these approaches for checking the effectiveness of a resonator using the lumped parameter approach in which the resonator was considered as a mass (neck), and a spring (cavity) system, and where the expression for the resonator frequency and the transmission loss was obtained. The resonators shown in figure 1.6 are often considered as spring mass systems for the convenience of analysis and for understanding behavior of Helmholtz resonators.

Figure 1.6: Helmholtz Resonator [26]

1.3 Motivations and Objectives

Helmholtz resonators have been studied extensively using different configurations as linear systems. However, the presence of excess average pressures inside the Helmholtz resonator lead to erroneous results when using linear stiffness and linear damping forces to simulate these resonators [51]. Therefore, nonlinear analysis became necessary [52-56].

This thesis focuses on nonlinear analysis of a special type of Helmholtz resonators which includes a neck-volume-neck- volume in series arrangement (Dual Helmholtz Resonators). This type of resonator provides a necessary solution for attenuating the noise at two distinct frequencies. This is needed when using ducted rotating machineries with varying loads [37]. The objectives of this thesis are

1. Analyzing acoustic behaviors of Helmholtz resonators with different configurations, and comparing their acoustic characteristics using linear and nonlinear approaches.
2. Studying the effect of a Helmholtz resonator's dimensions on its effectiveness of noise attenuation.
3. Analyzing softening and hardening behaviors of Helmholtz resonators under different sound pressure levels.
4. Studying the possibility and feasibility of activating energy transfer by using a dual Helmholtz resonator having nonlinear properties.

1.4 Thesis Organization

This thesis is divided into five chapters as follows:

- **Chapter 1: Introduction:** This chapter introduces the topic investigated in the thesis. It provides an introduction about acoustic resonators, followed by some information about wave equations and then the research objectives of the thesis.

- **Chapter 2: Literature Review:** This chapter reviews the literature on Helmholtz resonators with different configurations including:
  - Single Helmholtz Resonators
  - Multiple Helmholtz Resonators
  - Linear and Nonlinear Helmholtz Resonators.
- **Chapter 3: Mathematical Analysis of Linear HHR Configurations:** This chapter presents the analysis of acoustic attenuation due to different configurations of single and dual HHRs studied linearly. Numerical solutions are carried out for each case on the resonance frequencies and the change of transmission loss as a function of the demonstrated area ratio and the length of the Helmholtz resonator. Also, the possibility of chaos is examined for each case using a bifurcation diagram and phase portraits. Frequency and time history are also obtained.
- **Chapter 4: Mathematical Analysis of Nonlinear HHR Configurations:** This chapter presents the analysis of acoustic attenuation due to different configurations of single and dual HHRs studied nonlinearly. Numerical solutions are carried out for each case on the frequency and time history as well as the possibility of chaos using a bifurcation diagram and phase portraits. Frequency and time history are obtained, and the results are compared with the ones that belong to the linear system. Then, the possibility for activating a targeted energy transfer is investigated using a Kundt tube with single and dual HHR.

- **Chapter 5: Conclusions and Recommendations:** This chapter concludes and summarizes the work that has been carried out in the thesis against the objectives set for the study. Also, some recommendations are highlighted based on the obtained results.

CHAPTER 2

LITERATURE REVIEW

2.1 Chapter overview

Related research on the aspects of the Helmholtz resonators acoustic attenuator is discussed. These studies are categorized into three general research directions which are: single Helmholtz resonators, multiple Helmholtz resonators, as well as the linear and nonlinear systems of Helmholtz resonators.

2.2 Background

A Helmholtz oscillator or Helmholtz resonator is one of the simplest models in acoustic research and engineering applications. Its simplicity and effectivity is to directly apply the theoretical formula for its resonance frequency of formulation. It consists of a container of fluid which is called the (cavity) with an open hole (neck) because of the 'springiness' phenomena of air inside the cavity where the vibration occurs at the entrance of the neck. A Helmholtz resonator can be found in different life applications such as the common system of an empty bottle and the air in the body of a guitar [19].

2.2.1 Single Helmholtz Resonators

Helmholtz resonators are the simplest and most common type of noise suppressors, and their design has a cavity, which communicates or is connected with external ducts through the neck or orifice. This provides a reduction for the noise centralized in a narrow band which is in its resonance frequency range. The design variation can provide the

change in different ranges of frequency; therefore it is possible that, based on geometry, the design of an HHR can be made based on the desired resonance frequency [8].

Due to the unique tunable and durable characteristics of a Helmholtz resonator, it is being used in various types of duct structure systems which includes the HVAC systems most commonly used in buildings and industrial units, the duct systems in automobiles, and the engines of airplanes, for the reduction of noise as per the requirement [9]. Moreover, the applications of Helmholtz extend to other research areas, including cloak-based acoustic materials and special ultrasonic based meta-materials [10].

The first mathematical based theory for the Helmholtz resonator was established in the 18^{th} century to discuss and explain the phenomena of the wave occurring in the resonator. The Rayleigh made this theory more convenient and simple to understand [11].

One additional feature of the Helmholtz resonator is that it has its own natural frequency which is dependent on the dimensional parameters which include the length and diameter of the neck, along with the volume of the cavity [12]. The only issue with the Helmholtz resonator is that their reliability is less than the other acoustical devices like baffles, although one advantage over other systems is that it can be installed as a secondary system without interrupting and making any significant changes in the design of the duct or the noise containing system. A comparison study of Helmholtz resonators, a half-wave resonator, and a quarter-wave resonator, for the same resonant frequency and the same throat diameter provided us with the conclusion that Helmholtz resonators are more

effective in terms of absorption [13]. Based on the simplicity associated with a one-dimensional analytical approach, many studies have been done to analyze the suppressing properties of sound waves. Then there comes the non-planar propagation of waves in both the neck and cavity region which requires a multi-dimensional approach This approach has been employed to predict the sound attenuation in Helmholtz resonators with many geometries, including a concentric type circular cavity, circular symmetric-based cavity, enhanced neck length and lined absorbing material [14]. Many existing passive control systems are being used in the acoustical fields, including porous materials, resonators, and viscoelastic materials which are all efficient at high and medium frequency ranges. For low-frequency noise control, only a few of them are applicable. Therefore, to have effective control of low-frequency noises, a Helmholtz resonator is considered the best option [15]. Although they only use a narrow band of frequencies, they are adjustable by design. Several types of variations that exist in Helmholtz resonators have been studied [16]. Kumar and Rienstra [17] have shown that, in a Helmholtz resonator, linear dissipation exists due to the thermos viscous based boundary layers and the dissipation due to the nonlinearity that comes from vortex shedding. In addition, it was also shown that vortex apparition and dissipation around the neck could be highly affected by the dimensional parameter of the neck. This proved that it could also be possible to go further into the nonlinear domain, in the concept of restoring forces, which have a nonlinear effect. Some of the authors have also modelled this phenomenon by either considering the damping or restoring force in nonlinear together or separately. This work has been further studied by Yu et al. [18] who showed that, for nonlinear damping, we could consider the jet loss as

the reason and the nonlinear elasticity of the cavity air as the restoring force due to the high amplitude excitations.

2.2.2 Multiple Helmholtz Resonators

One addition to the fantastic concept of Helmholtz resonators are Multiple Helmholtz Resonators in which the resonators are combined to together for the enhancement of the attenuation effect in the wave guiding duct. The resonators are often considered by researchers as a lumped system if the dimensions of the HR are smaller than the acoustical wavelength [33].

For a single resonator we have the following parameter based variations which are length, shape, and perforations and the change in these parameters provide us with control over resonance frequency and control over the transmission loss as studied by Selamet A. and Lee IJ [12], who have also studied the effect of the thickness and density of the fibrous material [34]. However, when these parameters are considered in multi-couple resonators the variation possibility increases, improving our control not only in the two resonance frequency region, but in the entire spectrum of that region by changing the design.

Any spectral of the tonal wave does not just consist of one narrow band of frequency, instead it has a wide range of frequencies which needs to be suppressed by multiple resonators connected together. The Dual Helmholtz can have many configurations, and they can consist of multiple types, either in the form of serial arrays or parallel arrays. When Helmholtz has a configuration in the form of a neck-cavity neck – cavity on the duct it is called as Serial HR Array. If the Resonators are mounted in the same cross-section of

the duct, they are called parallel arrays [35]. Griffin et al. [36] utilize the concept of parallel Helmholtz resonators, in which two resonators were connected by the throats with a membrane in between, and the membrane position is changed to cover the range of narrow frequency bands based on the position resulting in proving a broad bandwidth attenuation.

The coupled resonators system was also implemented with an active feedback technique, but it has size limitations and cannot be accommodated in compact systems [29]. Hawwa [37] in his work introduced the unique concept of covering the space limitation by having both single and multiple coupled resonators as per our desire, along with an active control mechanism. He designed a structure in which we have two structures of resonators; one is movable while the other is immovable. The movable one is attached to a duct and has an open neck on top and on it, there are two c-channels on which the movable one slides. It has a flat plate underneath an active feedback mechanism which converts into either a single or dual based system depending on the spectrum attenuation requirements.

The solutions were previously based on the simplified closed form expression, but with further research it was seen that for attenuation analysis, acoustic performance needs to be established and the solution is to consider the analytical expressions for both the resonance frequency and the transmission loss and to use the pressure/ velocity matching technique. This was solved by the analytical method by Selamet [14].

Chenhzi et al. [35] studied the Dual Helmholtz resonators with both series based and parallel based arrangements and realized the fact that, by altering the connected sequence

of two HRs in the dual HR, the reduced first resonance frequency which compromises an increasing second resonance frequency could be observed.

2.2.3 Linear and Nonlinear Helmholtz Resonators

Nonlinear regions are a particular type of regions and their derivation or equations cannot be based on the conventional based asymptotic solutions. Also they cannot provide impedance close to resonance when studied in the linear regions [17]. Although linear regions which contain one form equations, or which can be derived merely with one-degree polynomial analysis, the same is not the case with nonlinear types where many forms of equations are included, and multiple degrees are added for the derivation of equations with the added advantage of more detailed analysis.

Nonlinear characteristics have always been found to improve the system analysis either in the acoustic region, the fluid region or the electronics area. When Helmholtz studied with the analogy of Tuned Mass Dampers (TMD), they were only efficient for three specific frequencies in the linear region [39]. Gourdon et al. [38] showed in their work that, with the addition of cubic nonlinearity in the system restoring force, it allowed for controlling the vibration in a broader frequency range than when it is considered with the linear region having an analogy with TMD [38].

In another analogy, Nonlinear energy sinks were developed and found to be better than the linear ones because it was seen that they add minimal mass to the system and can oscillate with any frequency as not having the natural frequency, in comparison to the linear ones which add great mass to the system and which are effective only in narrow frequency

bands [40]. Manevitch el al. showed that the Nonlinear normal modes (NNM) are effective in the analysis of weaker energy exchange methods [41,42]. Singh et al. [17] modelled a Helmholtz HR considering the nonlinear damping term instead of the linear, but used it for the restoring force.

In another application for nonlinear effectiveness, Ture et al. [40] showed that, during the excitation of the structure, it was seen that nonlinear energy sinks in parallel when observed with nonlinear regimes. They controlled the targeted mode of the system very well as compared to the linear side, and not only from the phase and amplitude point of view, these two nonlinear sinks worked very well and allowed the main structure in question to behave in an acceptable and a controlled manner.

Förner et al. [16] explained several types of dissipations that exist in an HR. They argue that the linear dissipation comes from the thermo-viscous boundary layers and the nonlinear dissipation comes mainly from the vortex shedding [16,17] inward studies that orifice in a plate considering the acoustic nonlinearity, and found that in the linear regime which is for low amplitudes, for a low region the flow through the orifice is irrotational and at high amplitudes is the jet type (nonlinear regime).

Since nonlinearity analysis has shown that it is not only feasible for more detailed structure analysis, but its introduction in the system has provided the effective improvements which had not been possible in the linear regimes or linear based analysis. Many methods have been developed for analyzing nonlinear based systems. As discussed,

nonlinear systems can accommodate multiple degrees of freedom. Platten et al. used an extended modal space model for the identification of multiple degrees of freedom.

The nonlinear effects considered in acoustical systems are of hydro-dynamical origin because of vortex shedding at the opening outlet. This is a complicated process for accounting nonlinear effects and the physical inspired model was introduced for the nonlinear corrections that do not have much efficiency in solving the nonlinearity of nonlinear resonators. The concept of CFD simulations were applied in [43,44,45], but it was shown by Innes and Crighton [46] that if different configurations were used and high amplitudes were considered with grazing flow and a slightly different differential equation of motion, then nonlinear effects can be analysed. As a result, a nonlinear Helmholtz resonator equation of motion is analyzed systematically.

The nonlinearity, unlike the linear analysis, is based on both the Physical Perspective and Equation-based perspective. In the case of the physical perspective, if we take the geometry of HR to be fixed, for systematic equations the cubic and quadratic terms depend on the specific heat ratio. Therefore, softening and hardening depends on it. However, if the damping is too large, then the hardening behavior requires modification of the geometry to take into account this nonlinearity [38]. Alamo et al. [38], with the Nonlinear responses obtained during analysis, presented an idea of designing a pure acoustical resonator which is considered as the passive controller and also can be coupled with the main media, providing us the attenuation in a broader range of frequencies, which is used as nonlinear absorber in a mechanical vibrating system.

CHAPTER 3

MATHEMATICAL ANALYSIS OF LINEAR HHR CONFIGURATIONS

3.1 Introduction

In this chapter, the mathematical formulations of acoustic wave propagation in ducts with multiple configurations of HHRs is derived by applying linear analysis. Transmission loss and the resonance frequencies for each configuration is generated using MATLAB. The effect of the HHR dimensions and a comparison between the different configurations are made. Also, the possibility of chaos is examined for each case using a bifurcation diagram and phase portraits. Frequency and time history are also obtained.

The assumptions used to derive the basic equations of the acoustic models are listed as follows:

- Two-Dimensional Geometries.
- Fluid inside the Helmholtz resonator is air.
- Air Flow inside the resonator is negligible.
- Heat transfer through Helmholtz resonator is negligible.
- The acoustic absorptivity of Helmholtz resonator's inner surface is negligible.

3.2 Wave Equation

Sound waves in a particular medium are governed by the following equation for the acoustic pressure, p,

$$\frac{1}{\rho_0 c_0^2}\frac{\partial^2 p}{\partial t^2} + \nabla.\left(-\frac{1}{\rho_0}(\nabla p - Q)\right) = 0 \tag{3.1}$$

The combination $\rho_0 c_0^2$ is called the bulk modulus and Q represents the monopole source. In terms of the acoustical potential function $\emptyset$, the wave equation can also be written as [27]:

$$\nabla^2 \emptyset = \frac{1}{c_0^2}\frac{\partial^2 \emptyset}{\partial t^2} \tag{3.2}$$

3.2.1 Plane Waves

In the case of plane wave propagation, similar to figure 3.1 below, only one single dimension x is required to describe the acoustic field. One instance of a plane wave propagation is sound propagating at the center of a rectangular duct. In this case equation (3.2) written in terms of the potential function $\emptyset$ becomes:

$$\frac{\partial^2 \emptyset}{\partial x^2} = \frac{1}{c_0^2}\frac{\partial^2 \emptyset}{\partial t^2} \tag{3.3}$$

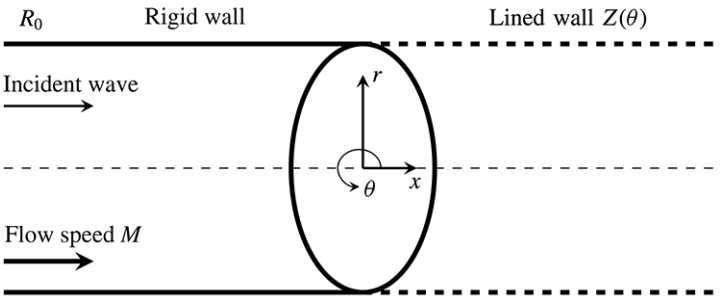

Figure 3.1: Plane Wave in a Duct [28]

3.3 Transmission Loss

Acoustic performance for silencer can be verified using three methods: either insertion loss (IL) or noise reduction (NR) or transmission loss (TL). The insertion loss is difference in sound levels measured between two rooms, before and after a barrier or silencer is installed, is referred to as Sound Insertion Loss, while the noise reduction is the process of removing noise from a signal and the transmission loss which is conducted throughout this chapter represents the difference between the sound pressure level between the incident waves entering and the transmitted waves exiting the silencer. Transmission loss is independent of the source and requires an anechoic termination at the downstream end.

The theoretical transmission loss is defined as the logarithmic ratio of incident to transmitted acoustic pressure amplitude into an anechoic termination as Equation 3.4 [27]:

$$TL = 20log_{10}\left|\frac{T_1}{T_2}\right| \tag{3.4}$$

Where T_1 and T_2 are the acoustic pressure of the incident wave in the inlet and outlet respectively.

3.4 Lumped Parameter Method

The term "lumped" comes from electrical engineering and refers to *lumped-parameter analysis.* It simplifies the description of the behavior of a combined system into a set of discrete components. In acoustics, as shown in figure 3.2, the capacitor is represented by a rigid-wall cavity and is proportional to its volume, while the conductor is proportional to the ratio of the length to the area of the neck. The resistor depends on the material's properties and dimensions. The loudspeaker can be represented by a series of zero-impedance voltage source, capacitor, inductor, and resistor. It is generally a recommended method if the object's dimensions are relatively much smaller than the wavelength of the incident wave. Consequently, there is a maximum limit of frequency to keep this method valid. Fortunately, the range of studied frequencies throughout the thesis is relatively small, which allows for applying the Lumped parameter method.

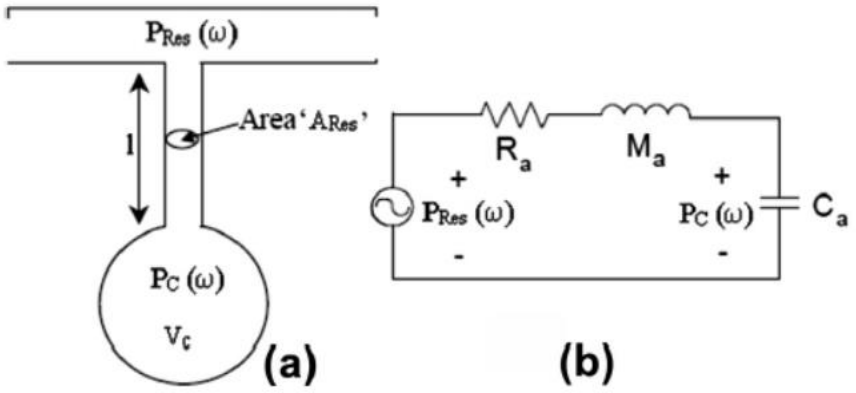

Figure 3.2: (a) Helmholtz Resonator and (b) Electric Analogy [30]

3.5 Chaos and Bifurcation

Scientists and researchers have given a great deal of attention to the chaotic behavior of nonlinear dynamical systems. This concentrate is attributable to losing consistency and the subsequent controllability of the dynamic frameworks. Among these dynamical frameworks, acoustical systems (including Helmholtz resonators) have a more extensive scope of applications and resulting research field. Chaos refers to an unusual phenomenon that is disorderly and irregular. In the modern scientific terminology, however, chaos has a rather precise but fairly complicated definition using the dynamics of a generally nonlinear system. For example, "in theoretical physics, chaos is a type of moderated randomness that, unlike true randomness, contains complex patterns that are mostly unknown". Vargas et al. [38] analyzed the dynamic behavior of a single Helmholtz resonator subjected to external pressure. They obtained a homoclinic orbit in a high dimensional amplitude. Chaotic motion of viscoelastic beams with physical nonlinearities

has been studied by Chen et al. [47]. They employed phase plane trajectory and power spectrum to define the chaotic behavior of the beam.

Bifurcation, as another scientific terminology, has been used to describe significant qualitative changes that occur in the trajectories of a generally nonlinear dynamical system. However, chaos is used more frequently than the bifurcation, but it is usually used to describe the qualitative stability changes of the trajectories of a nonlinear dynamical system [48].

In this chapter both phenomena is examined, as well as some related essential ones in the theory of linear dynamical systems, throughout different cases of linear systems.

Linear Modeling for Different Configurations of Helmholtz Resonators

Two different configurations of HHRs are studied in detail in the following sections:

1. Linear Modeling of a Single HHR.
2. Linear Modeling of a Dual HHRs Connected in Series.

3.6 Linear Analysis of Single Helmholtz Resonator

When a single neck-cavity system is attached to a duct side branch, as shown in figure 3.3, the side branch has both inertia and compliance. This acoustic system, a single Helmholtz resonator, can be treated as a simple mass-spring system.

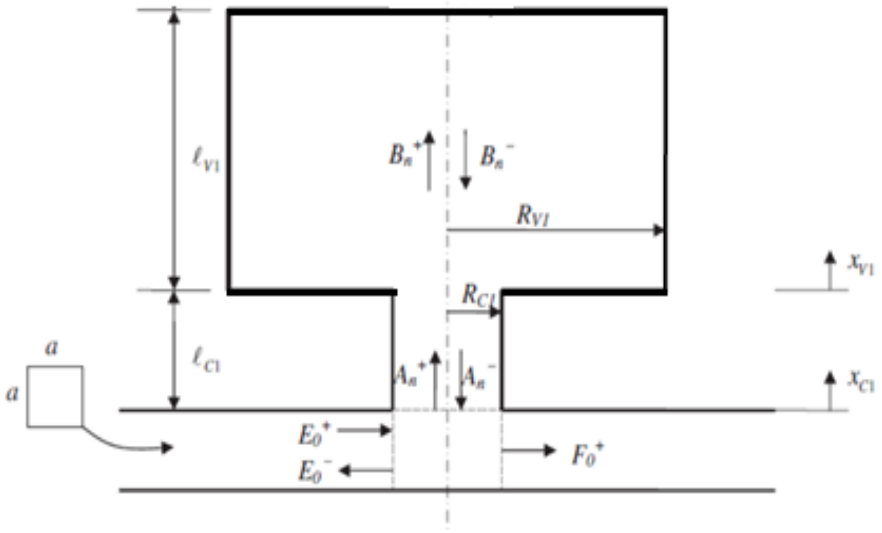

Figure 3.3: Single Helmholtz Resonator

3.6.1 Governing Equation of Motion of a Single Helmholtz Resonator

By applying Newton's second law on the neck and cavity system and assuming no damping in the system

$$m_1 \frac{d^2 x_{c1}}{dt^2} = \Delta p_1 A_{c1} = \frac{\Delta p_1}{\Delta \rho_1} \Delta \rho_1 A_{c1} \tag{3.5}$$

If a small variation is considered, then the difference in pressure and density values across the system can be written as below in equation (3.6)

$$\frac{dp_1}{d\rho_1} d\rho_1 A_{c1} = c_0^2 d\rho_1 A_{c1} = -c_0^2 \rho_0^2 A_{c1} dv_1 \tag{3.6}$$

Note that $m_1 = \rho A_{c1} \mathrm{L}_{c1}^{'} \; and \; \mathrm{L}_{c1}^{'} = L_{c1} + 16R_{c1}/3\pi$, while the difference in density is expressed as $d\rho_1 = -\rho_0^2 dv_1$. Then, combining

$$dv_1 = \frac{dV_1}{M_1} = \frac{A_{c1} x_{c1}}{M_1} \tag{3.7}$$

By rearranging equations (3.5) and (3.6), taken into account that $M_1 = \rho_0 V_1$, yield

$$\frac{d^2 x_{c1}}{dt^2} + \frac{c_0^2 A_{c1}}{L'_{c1} V_1} x_{c1} = 0 \tag{3.8}$$

Note that $V_1 = A_{v1} L_{v1}$ If the solution of the displacement is considered as $x_{C1} = X_{C1} e^{i\omega t}$ then by substituting this value into Eq. (3.8) the angular frequency ω reads as

$$\omega^2 - \left(\frac{A_{c1}}{L'_{c1} V_1}\right) c_0^2 = 0 \tag{3.9}$$

The resonance frequency for the dual Helmholtz resonator, could be found from the roots of equation (3.9), using the relation between the angular velocity (ω) and the frequency (f), gives

$$f = \frac{c_0}{2\pi} \sqrt{\frac{A_{c1}}{L'_{c1} V_1}} \tag{3.10}$$

3.6.2 Transmission Loss of Single Helmholtz Resonator

Transmission loss for single Helmholtz resonators is found by applying external pressure on the single DOF spring-mass system. As a result, after applying the pressure to the spring-mass system, the equation of motion below would be obtained:

$$m_1 \frac{d^2 x_{c1}}{dt^2} = -p A_{c1} - \frac{\rho_0 c_0^2 A_{c1}}{V_1} (A_{c1} x_{c1}) \tag{3.11}$$

Regarding the excitation force, based on the experiment conducted by Vergas et al. [38], where several experimental points were taken for a sound pressure level (SPL) excitation from 110 to 150 dB. The total pressure is defined as the sum of the atmospheric pressure p_0 and the fluctuation of pressure p; therefore, the expression of total pressure,

i.e., p_{tot}, is $p_{tot} = p_0 + p$. The excitation force is expressed using the fluctuation of pressure p. The ratio p/p_0 calculated for SPL = 110 dB and SPL = 150 dB is $p/p_0 = 6.2 \times 10^{-5}$ and $p/p_0 = 6.2 \times 10^{-3}$, respectively.

Substituting the solution of the displacement as well as for the external pressure as followings into equation (3.11): $x_{c1} = X_{c1}e^{i\omega t}$, and $-p = P_1 e^{i\omega t}$ into gives:

$$\mathbf{K}\{X_{C1}\} = [P_1 A_{c1}] \tag{3.12}$$

Where

$$\mathbf{K} = \left[-\mathrm{m}_1\omega^2 + \frac{\rho_0 c_0^2 A_1^2}{V_1}\right] \tag{3.13}$$

Then the transmission loss is expressed as

$$\mathrm{TL} = 20log_{10}\left|1 + \frac{A_{c1}}{2A_P}\frac{1}{ik\mathrm{L}'_{c1} + \frac{A_{c1}}{ikV_1}}\right| \tag{3.14}$$

Numerical Solution for the Transmission Loss

For a rectangular duct with (4.3cm x4.3cm) dimensions [14], table 3-1 shows the values of the HHR dimensions, which are selected to get the transmission loss.

Table 3-1: Physical Parameters for Single HHR with Linear Parameters [38]

No.	Dimensions	HHR
1	Radius of the Neck	3.0 mm
2	Length of the Neck	9.0 mm
3	Radius of the Cavity	42.2 mm
4	Length of the Cavity	21.5 mm
5	Speed of Sound	340.0 m/s
6	Density of Air	1.2 kg/m^3
7	Forced Frequency	(100~400) Hz
8	Incident Amplitude	(130~150) dB

The relation between transmission loss and frequency is plotted based on equation (3.14) as in the below figure which shows the resonance frequencies at 276 Hz.

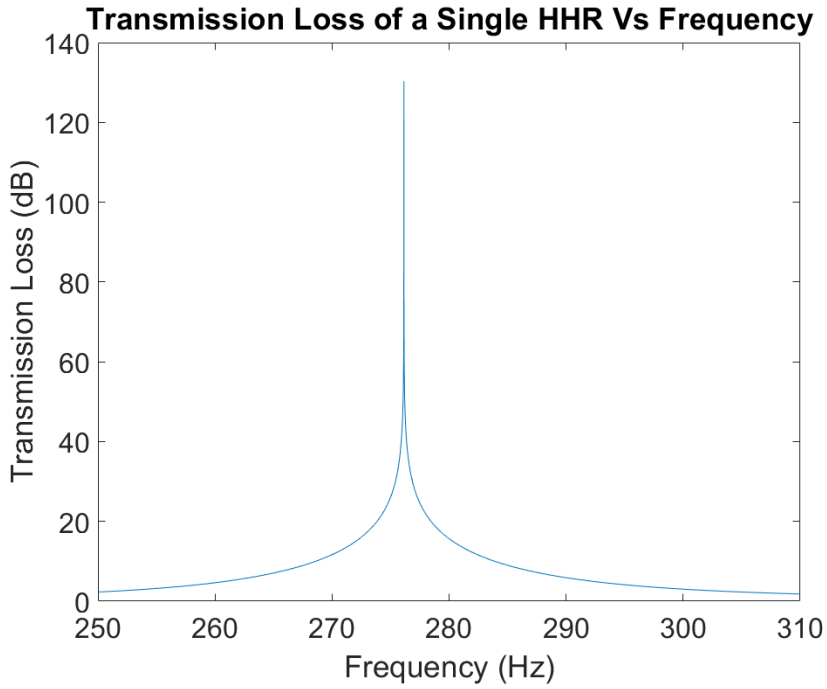

Figure 3.4: Transmission Loss of a Single Helmholtz Resonator

Figure 3.4 shows the transmission loss of a single Helmholtz Resonator. One transmission loss peak is observed at one resonance frequency (276 Hz). It should also be noted that the primary purpose of the above single HHR is to absorb the sound power in a low-frequency range.

Resonance Frequency and Tube Length

The HHR's neck-length is tuned to obtain the best resonance frequency as shown in figure 3.5.

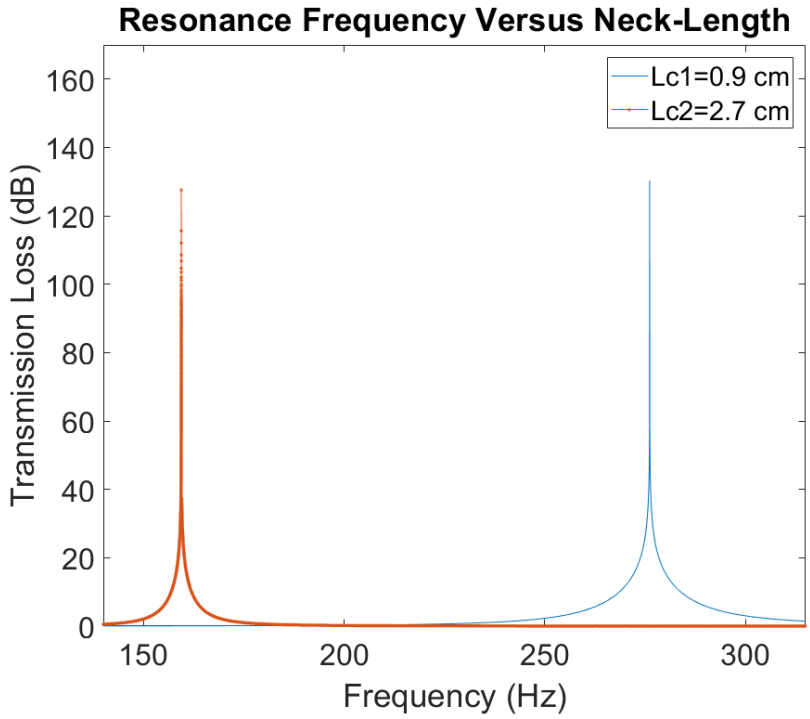

Figure 3.5: Resonance Frequency versus Neck Length

The original resonance frequency shifted from 276 Hz to 159 Hz, when the neck length is changed from 0.9 cm to 2.7 cm. As a result, the resonance frequency is inversely proportional to the length of the neck.

Resonance Frequency and Cavity Volume

The HHR's cavity volume is tuned to obtain the best resonance frequency as shown in figure 3.6.

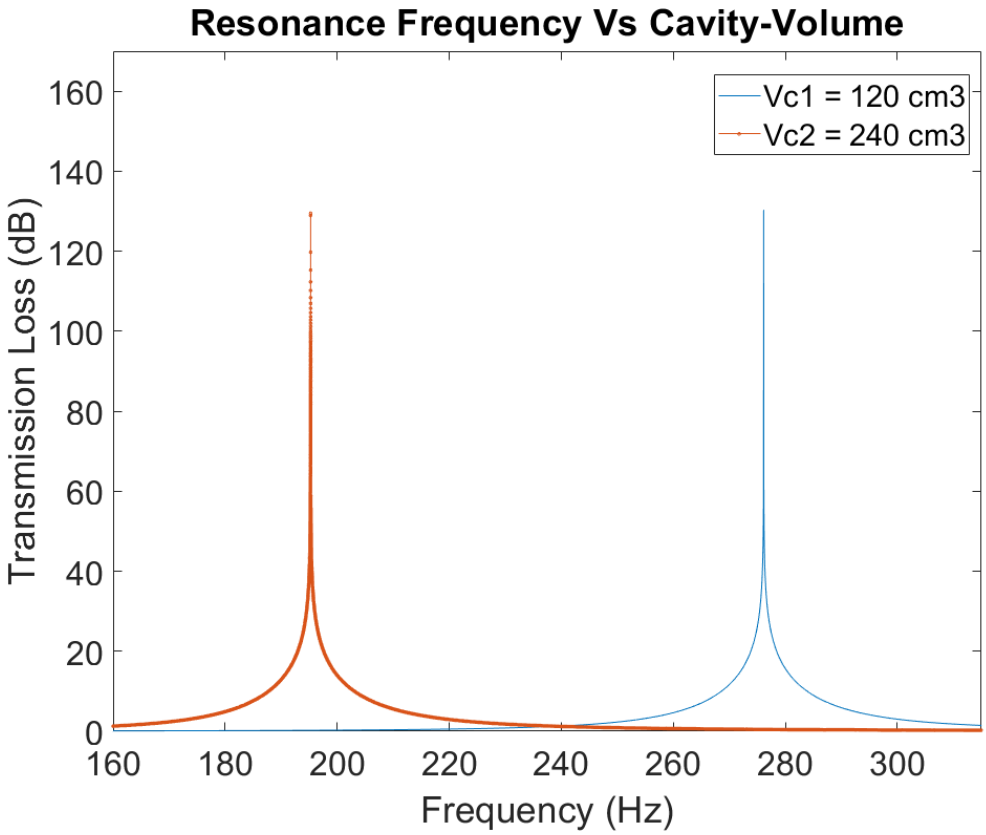

Figure 3.6: Resonance Frequency versus Cavity Volume

The original resonance frequency shifted from 276 Hz to around 195 Hz, when the cavity volume is increased from 120 cm^3 to 240 cm^3. As a result, the resonance frequency is inversely proportional to the volume of the cavity.

3.6.3 Possibility of Chaos

Perhaps surprisingly, chaos may occur in linear systems, provided they are infinite dimensional [50]. A theory of linear chaos is being developed in a branch of mathematical analysis known as functional analysis. In this section a bifurcation diagram and phase portraits are shown for a certain sound pressure level, after adding a damping term to

equation 3.11 to simulate a more accurate solution. The governing equation of motion becomes:

$$m_1 \frac{d^2 x_{c1}}{\mathrm{d}t^2} + \frac{2m_1 A_{c1}}{2\rho_0 \mathrm{L}'_{c1}} R(Z_{in} + Z_{vis}) \left(\frac{dx_{c1}}{dt}\right) + \frac{\rho_0 c_0^2 A_{c1}}{V_1} (A_{c1} x_{c1}) = -p\mathrm{A}_{\mathrm{c1}} \qquad (3.15)$$

Introducing dimensionless variables, t*=$\omega_0 t$, $x_1 = \frac{x_{c1} A_{c1}}{V_1}$, and assuming harmonic excitation sound wave with forced frequency (ω), we get:

$$\frac{d^2 x_1}{\mathrm{d}t^{*2}} + c_1 \left(\frac{dx_1}{dt^*}\right) + x_1 = P\, cos(\Omega t^*) \qquad (3.16)$$

where

$$\omega_0 = \frac{c_0^2 A_{c1}}{\mathrm{L}'_{c1} V_1} \qquad c_1 = \frac{\delta}{\omega_0} = \frac{2A_{c1}}{2\rho_0 \mathrm{L}'_{c1} \omega_0} R(Z_{in} + Z_{vis})$$

$$P = \frac{-p\mathrm{A}_{\mathrm{c1}}}{\rho_0 \mathrm{L}'_{c1} \omega_0^2 V_1} \qquad \Omega = \frac{\omega}{\omega_0}$$

where the linear damping coefficient δ equals 8.674 s^{-1} [38].

A) Bifurcation Diagram

The Bifurcation diagram shows the relation between the applied sound wave pressure level and the HHR displacement. Figure 3.7 shows that there is no possibility of chaos, even with very high sound pressure signal levels such as 150 dB.

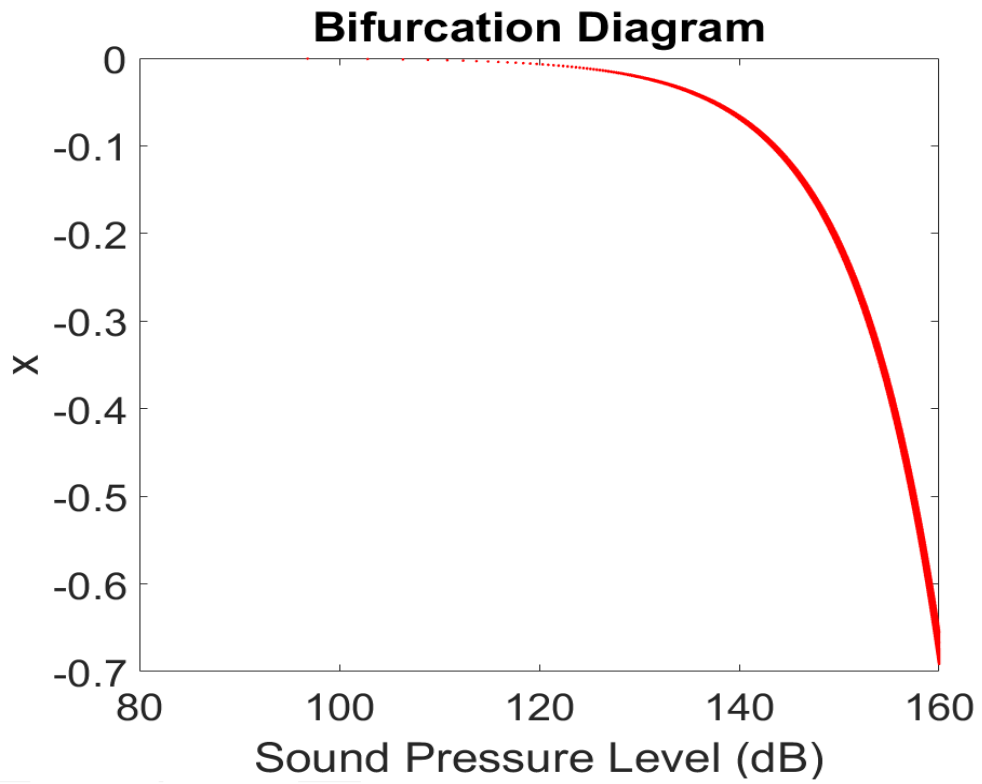

Figure 3.7: Bifurcation Diagram for Single HHR Analyzed Linearly with $\Omega = 1.01$

B) Phase Portraits

Phase Portraits of Linear Systems consider a linear homogeneous system. They describe the motion of a point in the plane, with the independent variable as displacement. Figure 3.8 describes the phase portraits for the single HHR after applying a sound wave of 150 dB.

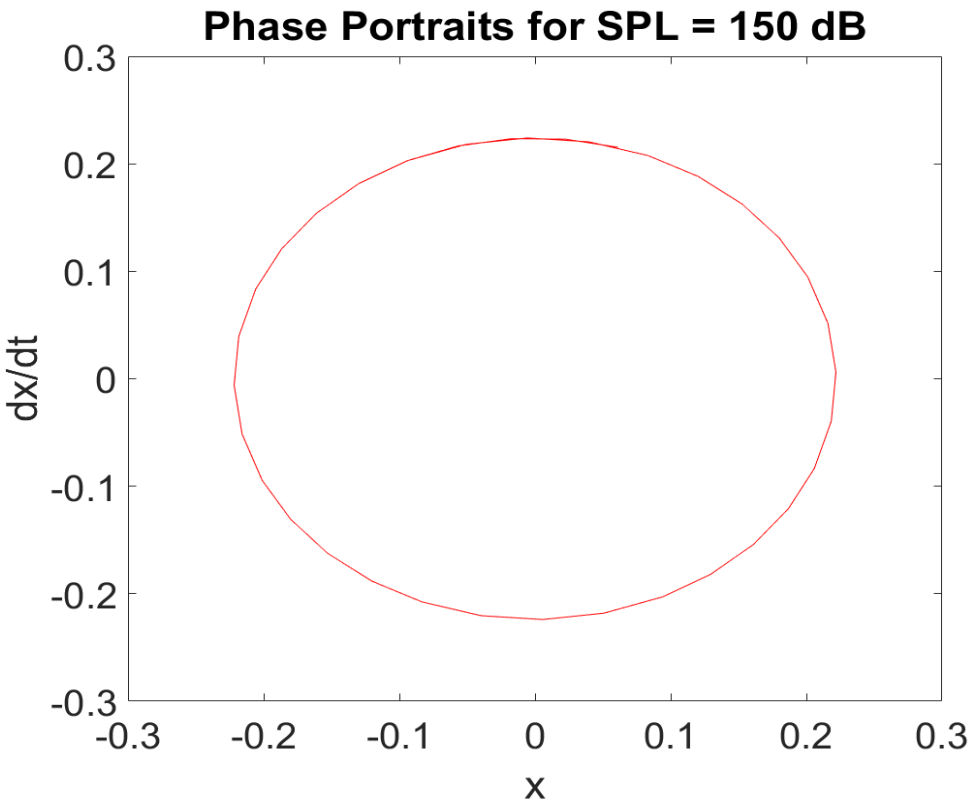

Figure 3.8: Phase Portraits for Single HHR Analyzed Linearly Excited by 150 dB

Figure 3.8 shows a purely periodic solution, which is consistent with the result observed from figure 3.7.

3.6.4 Frequency and Time History

Numerical simulations of the equation presented in figure 3.9 show the frequency history under different sound pressure levels.

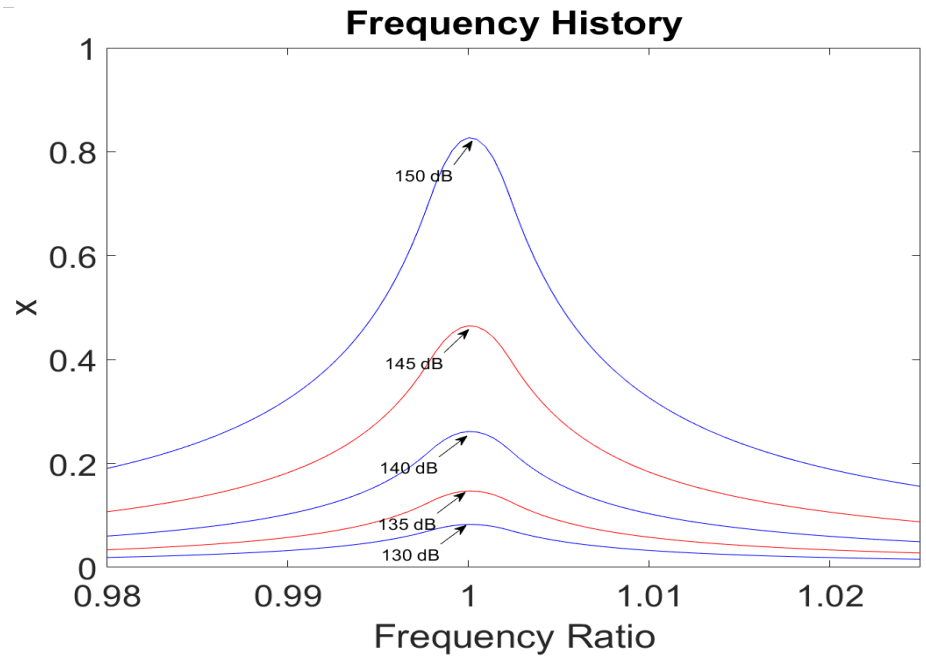

Figure 3.9: Frequency History for Single HHR Analyzed Linearly at Different SPL

Time history at sound pressure level of 150 dB is presented in figure 3.10 and shows a periodic behavior response.

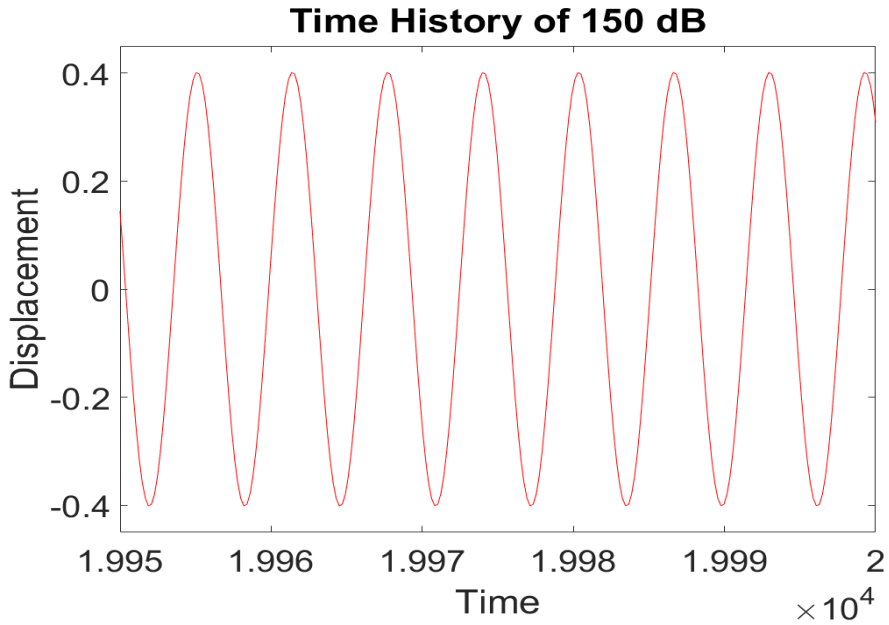

Figure 3.10: Time History for Single HHR Analyzed Linearly Excited by 150 dB

3.7 Linear Analysis of Dual Helmholtz Resonators

Dual Helmholtz resonators consist of a pair of neck and cavity connected on a series lead to two resonance frequencies which can create dual Helmholtz resonators and a desirable silencing element like the engine breathing system [14]. Similar to what has been analyzed in the single Helmholtz resonator, the acoustic properties including resonance frequencies and transmission loss for a dual HHR are shown in figure 3.11. Linear governing equation of motion is derived and investigated, before going for the possibility of chaos as well as frequency and time history.

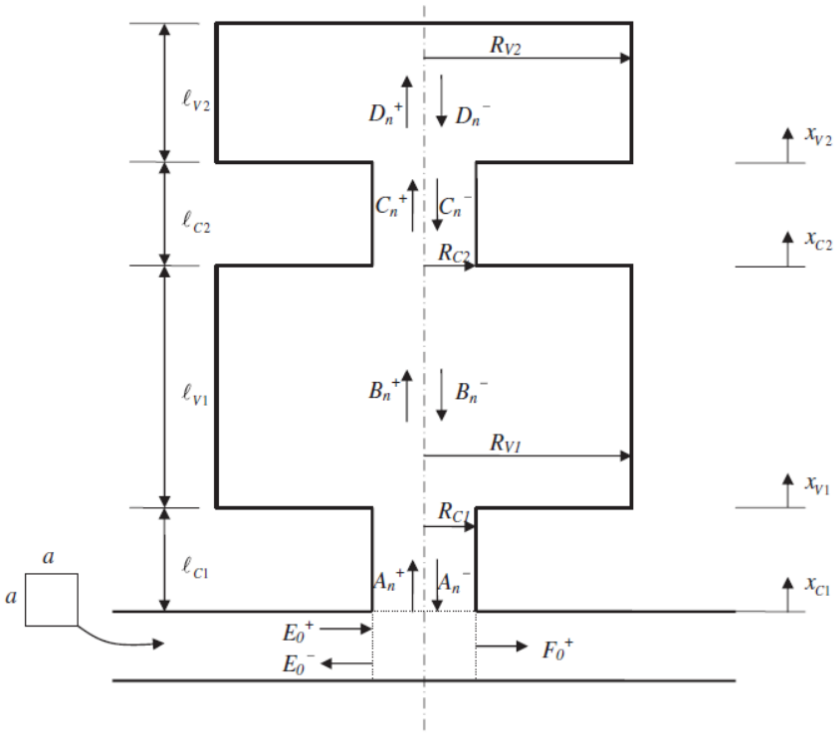

Figure 3.11: Dual Helmholtz Resonator [14]

3.7.1 Governing Equation of Motion for Dual Helmholtz Resonators

By applying Newton's second law on the first neck and cavity system.

$$m_1 \frac{d^2 x_{c1}}{dt^2} = \Delta p_1 A_{c1} = \frac{\Delta p_1}{\Delta \rho_1} \Delta \rho_1 A_{c1} \tag{3.17}$$

If a small variation is considered, then the difference in pressure and density values across the system can be written as below in equation (3.18)

$$\frac{dp_1}{d\rho_1} d\rho_1 A_{c1} = c_0^2 d\rho_1 A_{c1} = -c_0^2 \rho_0^2 A_{c1} dv_1 \tag{3.18}$$

Note that the difference in density can be expressed as $d\rho_1 = -\rho_0^2 dv_1$, and c_o stands for the speed of sound and considered 340.3 m/s as the fluid media is air. Then, combining

$$dv_1 = \frac{dV_1}{M_1} = \frac{A_{c1} x_{c1} - A_{c1} x_{c1}}{M_1} \tag{3.19}$$

By rearranging equations (3.17) and (3.18), taken into account that $M_1 = \rho_0 V_1$, yields

$$\frac{d^2 x_{c1}}{\mathrm{d}t^2} + \frac{c_0^2 A_{c1}}{L_{c1}' V_1} x_{C1} - \frac{c_0^2 A_{c2}}{L_{c1}' V_1} x_{c2} = 0 \tag{3.20}$$

Similarly, Newton's second law could be applied to the second neck-cavity system, which is working as a spring-mass system too, gives

$$m_2 \frac{d^2 x_{c2}}{\mathrm{d}t^2} = \Delta p_2 A_{c2} - \Delta p_1 A_{c2} = \frac{\Delta p_2}{\Delta \rho_2} \Delta \rho_2 A_{c2} - \frac{\Delta p_1}{\Delta \rho_1} \Delta \rho_1 A_{c2} \tag{3.21}$$

If a small variation is considered, then the difference in pressure and density values across the system is written as below in equation (3.22)

$$m_2 \frac{d^2 x_{c2}}{\mathrm{d}t^2} = -c_0^2 \rho_0^2 A_{c2} dv_2 + c_0^2 \rho_0^2 A_{c2} dv_1 \tag{3.22}$$

Substituting dv_1 from Eq. (3.19) and $dv_2 = \frac{dV_2}{M_2} = \frac{A_{c2} x_{C2}}{M_2}$ into Eq. (3.22) with

$M_2 = \rho_0 V_2$ and rearranging yields

$$\frac{d^2 x_{c2}}{dt^2} + \frac{c_0^2 A_{c2}}{L'_{c2} V_2} x_{c2} - \frac{c_0^2 A_{c1}}{L'_{c1} V_1} x_{c1} + \frac{C_0^2 A_{c2}}{L'_{c2} V_1} x_{c2} = 0 \tag{3.23}$$

Note that $m_2 = \rho A_{c2} L'_{c2}$ and $L'_{c2} = L_{c2} + 16R_{c2}/3\pi$, If the solution of the displacement is considered as $x_{c1} = X_{c1} e^{i\omega t}$ and $x_{c2} = X_{c2} e^{i\omega t}$ then by substituting these values into Eqs. (3.20) and (3.23), and combining them for the angular frequency ω gives

$$\omega^4 - \left(\frac{A_{c1}}{L'_{c1} V_1} + \frac{A_{c2}}{L'_{c2} V_1} + \frac{A_{c2}}{L'_{c2} V_2}\right) c_0^2 \omega^2 + \frac{A_{c1}}{L'_{c1} V_1} \frac{A_{c2}}{L'_{c2} V_2} c_0^4 = 0 \tag{3.24}$$

The resonance frequency for the dual Helmholtz resonator, could be found from the roots of equation (3.24), using the relation between the angular velocity (ω) and the frequency (f), gives

$$f_{1,2} = \frac{c_0}{2\sqrt{2}\pi} \sqrt{\left(\frac{A_{c1}}{L'_{c1} V_1} + \frac{A_{c2}}{L'_{c2} V_1} + \frac{A_{c2}}{L'_{c2} V_2}\right) \pm \sqrt{\left(\frac{A_{c1}}{L'_{c1} V_1} + \frac{A_{c2}}{L'_{c2} V_1} + \frac{A_{c2}}{L'_{c2} V_2}\right)^2 - 4 \frac{A_{c1}}{L'_{c1} V_1} \frac{A_{c2}}{L'_{c2} V_2}}} \tag{3.25}$$

Which could be expressed in terms of α_{21}, α_1 and V_{21}

$$\frac{f_{1,2}}{\frac{c_0}{2\pi}\sqrt{\alpha_1}} = \frac{1}{\sqrt{2}} \sqrt{1 + \alpha_{21}(1 + V_{21}) \pm \sqrt{[1 + \alpha_{21}(1 + V_{21})]^2 - 4\alpha_{21}}} \tag{3.26}$$

While $\alpha_1 = \frac{A_{c1}}{L'_{c1} V_1}$, $\alpha_2 = \frac{A_{c2}}{L'_{c2} V_2}$, $\alpha_{21} = \frac{\alpha_2}{\alpha_1}$ and $V_{21} = \frac{V_2}{V_1}$ as

If there is only one cavity and neck, then $\alpha_{21} \to 0$ and the default resonance frequency is found from equation (3.10) as

$$f = \frac{c_0}{2\pi} \sqrt{\alpha_1} \tag{3.27}$$

3.7.2 Transmission Loss of Dual Helmholtz Resonator

Transmission loss for the dual Helmholtz resonators is found by applying external pressure on the 2 DOF spring-mass system. Consequently, after applying the pressure to the first spring-mass system, which is identified in section 3.6.2, the following two equations are obtained:

$$\mathrm{m}_1 \frac{\mathrm{d}^2 x_{c1}}{dt^2} = -p\mathrm{A}_{c1} - \frac{\rho_0 c_0^2 A_{c1}}{V_1}(A_{c1}x_{C1} - A_{c2}x_{c2}) \tag{3.28}$$

$$\mathrm{m}_2 \frac{\mathrm{d}^2 x_{c2}}{dt^2} = \frac{\rho_0 c_0^2 A_{c2}}{V_1}(A_{c1}x_{c1} - A_{c2}x_{c2}) - \frac{\rho_0 c_0^2 A_{c2}^2}{V_2} x_{c2} \tag{3.29}$$

Substituting the solution of the first and second displacements as well as for the external pressure as followings into equations (3.28) and (3.29): $x_{c1} = X_{c1}e^{i\omega t}$, $x_{c2} = X_{c2}e^{i\omega t}$, and $-p = P_1 e^{i\omega t}$ gives:

$$\mathbf{K}\begin{Bmatrix} X_{c1} \\ X_{c2} \end{Bmatrix} = \begin{bmatrix} P_1 A_{c1} \\ 0 \end{bmatrix} \tag{3.30}$$

Where

$$\mathbf{K} = \begin{bmatrix} k_{11} & k_{12} \\ k_{21} & k_{22} \end{bmatrix} = \begin{bmatrix} -\mathrm{m}_1\omega^2 + \dfrac{\rho_0 c_0^2 A_{c1}^2}{V_1} & -\dfrac{\rho_0 c_0^2 A_{c1}A_{c2}}{V_1} \\ -\dfrac{\rho_0 c_0^2 A_{c1}A_{c2}}{V_1} & -\mathrm{m}_2\omega^2 + \rho_0 c_0^2 A_{c2}^2\left(\dfrac{1}{V_1} + \dfrac{1}{V_2}\right) \end{bmatrix} \tag{3.31}$$

is the stiffness matrix. By manipulating Eq. (3.31),

$$\frac{X_{c1}}{P_1 A_{c1}} = \frac{k_{22}}{k_{11}k_{22} - k_{12}k_{21}}, \frac{X_{c2}}{P_1 A_{c1}} = \frac{-k_{12}}{k_{11}k_{22} - k_{12}k_{21}} \tag{3.32}$$

Identifying the specific acoustic impedance for the Helmholtz resonator Z_H as

$$Z_H = \frac{p}{\rho_0 c_0 u_{C1}} = \frac{1}{i\omega\rho_0 c_0}\frac{P_1}{X_{c1}} = \frac{1}{i\omega\rho_0 c_0 A_{c1}}\frac{k_{11}k_{22} - k_{12}k_{21}}{k_{22}} \tag{3.33}$$

which yields the transmission loss of the dual Helmholtz resonator, as

$$TL = 20log_{10}\left|1 + \frac{A_{c1}}{2A_P}\frac{1}{Z_H}\right| \tag{3.34}$$

Then, the transmission loss is expressed as

$$TL = 20log_{10}\left|1 + \frac{A_{c1}}{2A_P}\frac{1}{ik\text{L}'_{c1} + \frac{A_{c1}}{ikV_1}\left(1 - \frac{A_{c2}V_2}{A_{c2}V_2 + A_{c2}V_1 - V_1V_2k^2\text{L}'_{c2}}\right)}\right| \tag{3.35}$$

Alternatively, by rearranging,

$$TL = 20log_{10}\left|1 + i\frac{A_{c1}}{2A_P}\left\{k\text{L}'_{c1}\left[-1 + \frac{\alpha_1}{k^2}\left(1 - \frac{1}{1 + \frac{1}{V_{21}} - \frac{k^2}{\alpha_2}\frac{1}{V_{21}}}\right)\right]\right\}^{-1}\right| \tag{3.36}$$

Numerical Solution for Transmission Loss

For a rectangular duct with (4.3cm x 4.3cm) dimensions, table 3-2 describes the parameters of the HHRs which are considered to plot the TL response.

Table 3-2: Physical Parameters for Dual HHR with Linear Parameters

No.	Dimensions	First HHR	Second HHR
1	Radius of the Neck	3.0 mm	3.0 mm
2	Length of the Neck	9.0 mm	9.0 mm
3	Radius of the Cavity	42.2 mm	42.2 mm
4	Length of the Cavity	21.5 mm	21.5 mm
5	Speed of Sound	340.0 m/s	
6	Density of Air	1.2 kg/m^3	
7	Forced Frequency	(100~700) Hz	
8	Incident Amplitude	(130~150) dB	

The relation between transmission loss and frequency is plotted based on equation (3.36) in figure 3.12, which shows the resonance frequencies at (171 and 447) Hz.

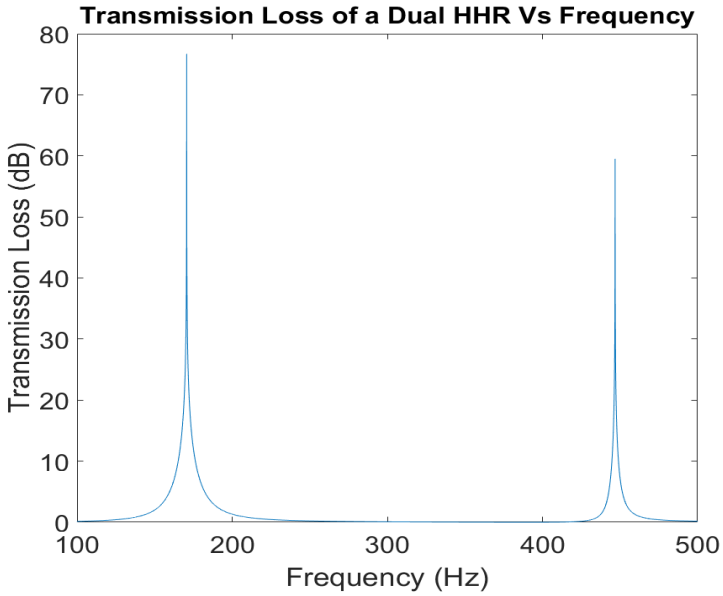

Figure 3.12: Transmission Loss of Dual HHR Analyzed Linearly

Figure 3.12 shows the transmission loss of a dual Helmholtz Resonator. Two transmission loss peaks are observed at two resonance frequencies (171 Hz and 447 Hz). As mentioned in the literature before, the main purpose of the dual HHRs is to absorb the sound power level at certain two- resonance frequencies located at a low-frequency range (i.e. Below 1000 Hz).

Resonance Frequency and Helmholtz Resonators-Area Ratio

The ratio of the first to second-neck area ($\frac{A_{c1}}{A_{c2}}$) controls the range of the attenuation frequencies and the level of transmission loss. In some applications, the required design areas of the first neck should be smaller than the other, while in different cases it might be vice versa.

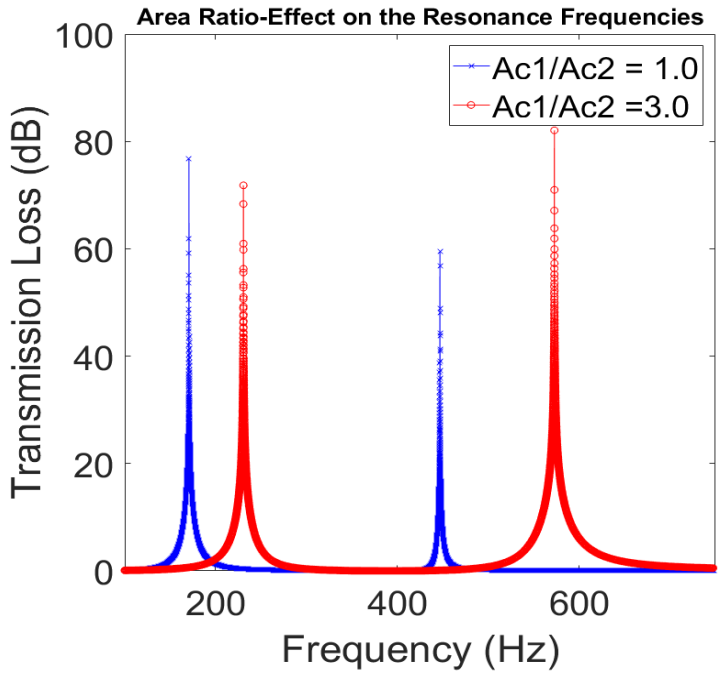

Figure 3.13: Resonance Frequencies versus Area Ratio of Dual HHR Analyzed Linearly

From figure 3.13, it is observed that the range of the resonance frequencies is proportional to the increase of the area ratio.

3.7.3 Possibility of Chaos

Chaotic behavior is not preferred, as it represents unpredictable behavior of the system. Therefore, we have to examine the appearance of such behavior using a bifurcation diagram, as well as phase portraits similar to the ones obtained in section 3.6. In order to simulate a more practical system, damping terms are added to equations 3.20 and 3.23, which becomes like equations 3.37 and 3.38, respectively.

$$\mathrm{m}_1 \frac{\mathrm{d}^2 x_{c1}}{dt^2} + \frac{2\mathrm{m}_1 A_{c1}}{2\rho_0 \mathrm{L}'_{c1}} \left(\frac{dx_{c1}}{dt} - \frac{dx_{c2}}{dt}\right) + \frac{\rho_0 c_0^2 A_{c1}}{V_1} (A_{c1} x_{C1} - A_{c2} x_{c2}) = -p\mathrm{A}_{\mathrm{c1}} \tag{3.37}$$

$$\begin{aligned} &\mathrm{m}_2 \frac{\mathrm{d}^2 x_{c2}}{dt^2} + \frac{2m_1 A_{c1}}{2\rho_0 \mathrm{L}'_{c1}} R(Z_{in} + Z_{vis}) \left(\frac{dx_{c2}}{dt} - \frac{dx_{c1}}{dt}\right) \\ &+ \frac{\rho_0 c_0^2 A_{c2}}{V_1} (A_{c2} x_{c2} - A_{c1} x_{c1}) + \frac{\rho_0 c_0^2 A_{c2}^2}{V_2} x_{c2} \\ &+ \frac{2m_2 A_{c2}}{2\rho_0 \mathrm{L}'_{c2}} R(Z_{in} + Z_{vis}) \left(\frac{dx_{c2}}{dt}\right) = 0 \end{aligned} \tag{3.38}$$

Introducing dimensionless variables, t*=$\omega_{01} t$, $x_1 = \frac{x_{c1} A_{c1}}{V_1}$, $x_2 = \frac{x_{c2} A_{c2}}{V_2}$ and assuming harmonic excitation sound wave with forced frequency (ω), we get:

$$\frac{d^2 x_1}{\mathrm{d}t^{*2}} + c_1 \left(\frac{dx_1}{dt^*} - \frac{A_{c1} V_2}{A_{c2} V_1} \frac{dx_2}{dt^*}\right) + (x_1 - \frac{V_2}{V_1} x_2) = P\ cos(\Omega t^*) \tag{3.39}$$

$$\frac{d^2x_2}{\mathrm{d}t^{*2}} + r_1c_1\left(\frac{dx_2}{dt^*} - \frac{A_{c2}V_1}{A_{c1}V_2}\frac{dx_1}{dt^*}\right) + \frac{\mathrm{L}_{c1}}{\mathrm{L}_{c2}A_{c1}}(A_{c2}x_2 - \frac{A_{c2}V_1}{V_2}x_1) + c_2\frac{dx_2}{dt^*} + r_2^2x_2 = 0 \quad (3.40)$$

Where

$$\omega_{01} = \frac{c_0^2A_{c1}}{\mathrm{L}_{c1}V_1} \qquad P = \frac{-p\mathrm{A}_{\mathrm{c1}}}{\rho_0\mathrm{L}_{c1}\omega_{01}^2V_1}$$

$$\omega_{02} = \frac{c_0^2A_{c2}}{\mathrm{L}_{c2}V_2} \qquad \Omega = \frac{\omega}{\omega_{01}}$$

$$c_1 = \frac{\delta_1}{\omega_{01}} = \frac{2A_{c1}}{2\rho_0\mathrm{L}_{c1}\omega_{01}}R(Z_{in} + Z_{vis}) \qquad r_1 = \frac{m_1}{m_2}$$

$$c_2 = \frac{\delta_2}{\omega_{01}} = \frac{2A_{c2}}{2\rho_0\mathrm{L}_{c2}\omega_{01}}R(Z_{in} + Z_{vis}) \qquad r_2 = \frac{\omega_{02}}{\omega_{01}}$$

Note that $\delta_1 = \delta_2 = 8.674\ s^{-1}$.

A) Bifurcation Diagram

Figure 3.14 shows that a homoclinic orbit does not exist for the applied range of sound pressure level, which indicates that there is no possibility of chaos at this range.

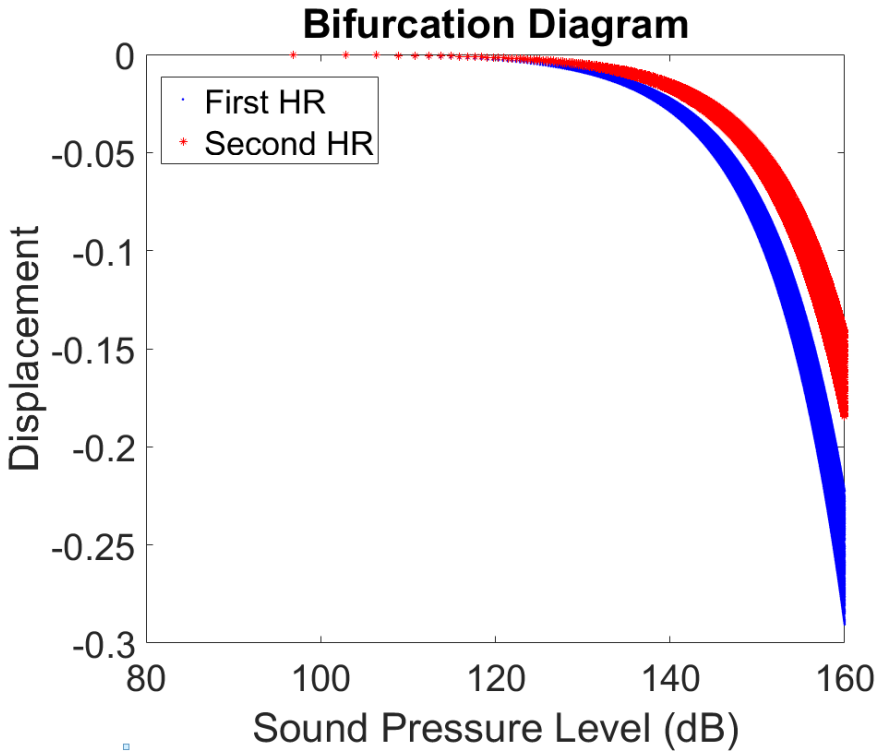

Figure 3.14: Bifurcation Diagram for Dual HHR Analyzed Linearly with $\Omega = 1.01$

B) Phase Portraits

The phase portrait shown in figure 3.15 is plotted based on a 150 dB sound pressure level. It is observed that there is a clear periodic behavior even at this ultimate pressure level.

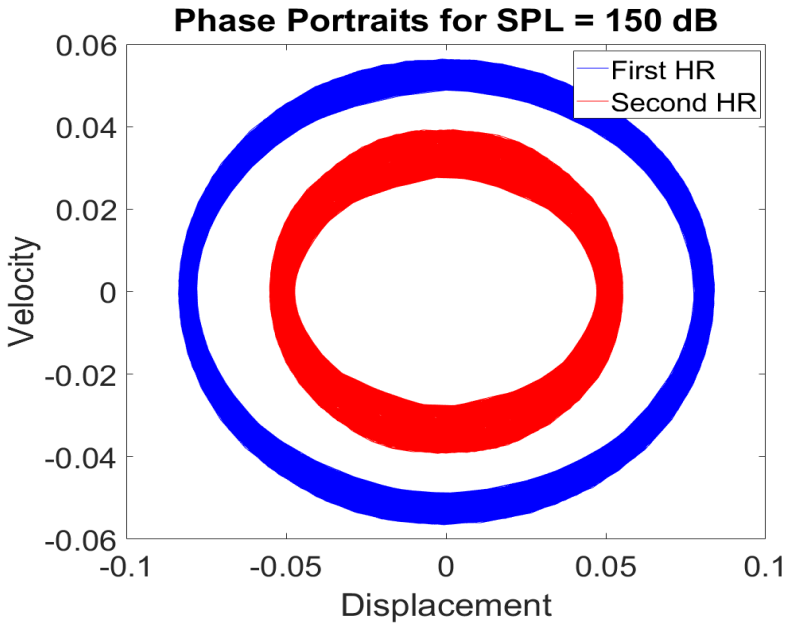

Figure 3.15: Phase Portraits for Dual HHR Analyzed Linearly Excited by 150 dB

3.7.4 Frequency and Time History

Numerical simulations of equations (3.39) and (3.40) are simulated for two different cases to examine the effect of the HHRs dimensions on the resonance frequency, as well as the displacement. The two different cases are:

1. Identical Masses and Volumes for both Helmholtz Resonators.
2. Identical Masses for both Helmholtz Resonators, While the Volume of the Second HHR-Cavity is double the Volume of the First HHR-Cavity.

For the case of identical dimensions for both HHRs, the frequency history is shown in figure 3.16, where the first and second resonance frequencies occur at a frequency ratio of 0.65 and 1.65, respectively. Also, the magnitude of displacement reaches 2.75 at the first resonance frequency. However, the magnitude of the second HHR displacement at the second resonance frequency is larger than the first HHR one.

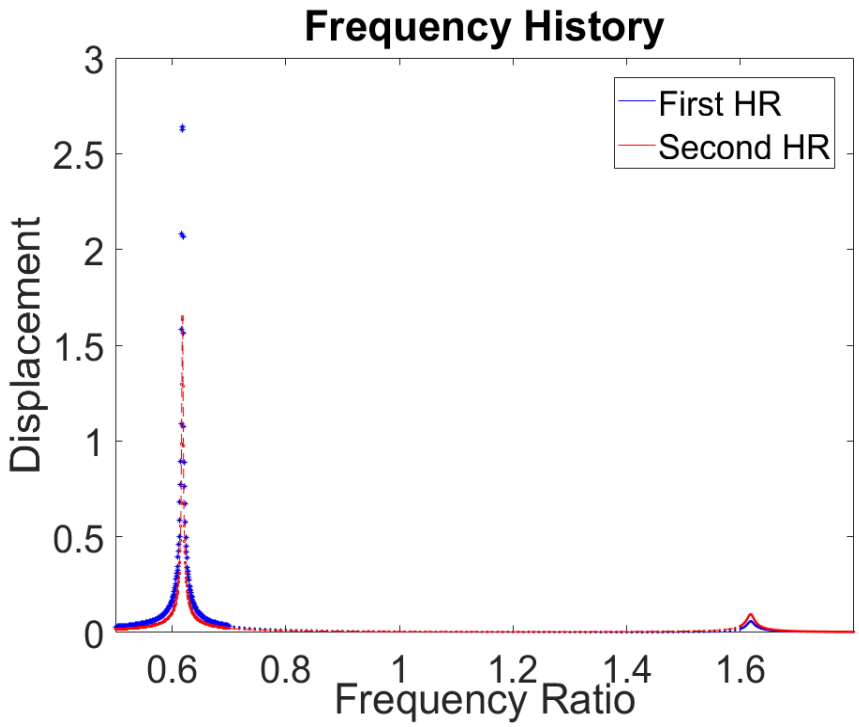

Figure 3.16: Frequency History for Dual HHR Analyzed Linearly (First Case)

Time history at the first and second resonance frequencies are shown in figures 3.17 (a) and (b) respectively.

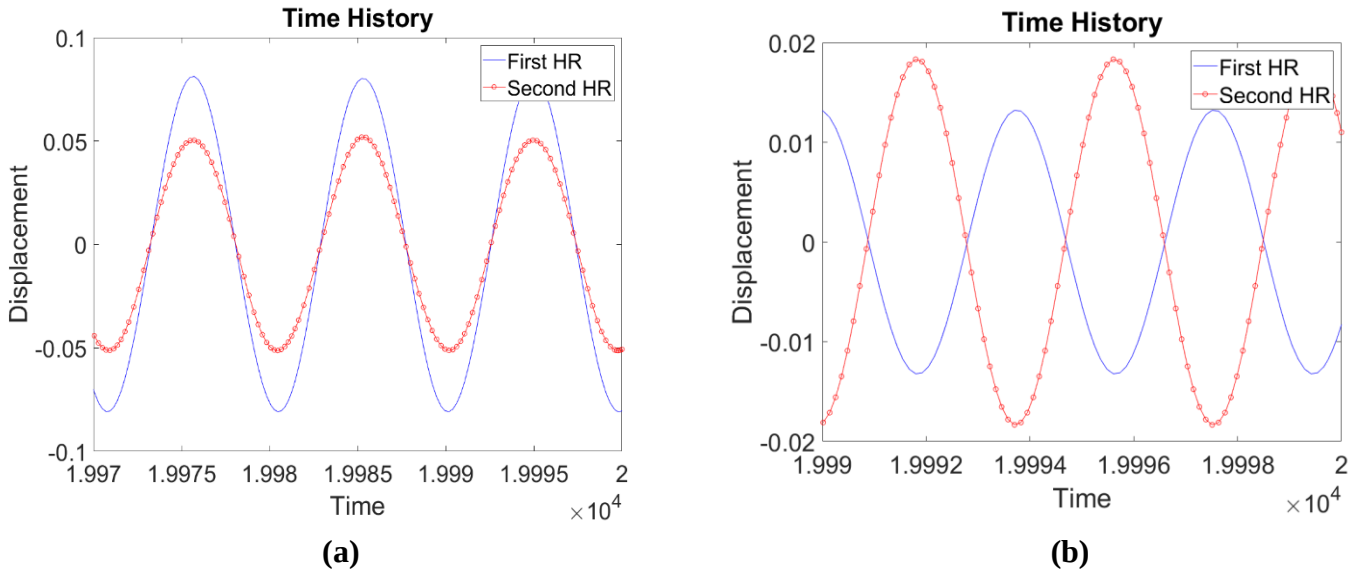

(a) **(b)**

Figure 3.17: Time History for Dual HHR Analyzed Linearly (First Case) at (a) Frequency Ratio = 0.65 (b) Frequency Ratio = 1.65

For the second case where ($m_1 = m_2$ and $V_2 = 2V_1$), the frequency history is shown in figure 3.18, where the first and second resonance frequencies occur at a smaller frequency ratio (0.45 and 1.55), respectively. Also, the magnitude of displacement only reaches 2.15 at the first resonance frequency. Also, contrary to the first case, the magnitude of the first HHR displacement at the second resonance frequency is larger than the second HHR one.

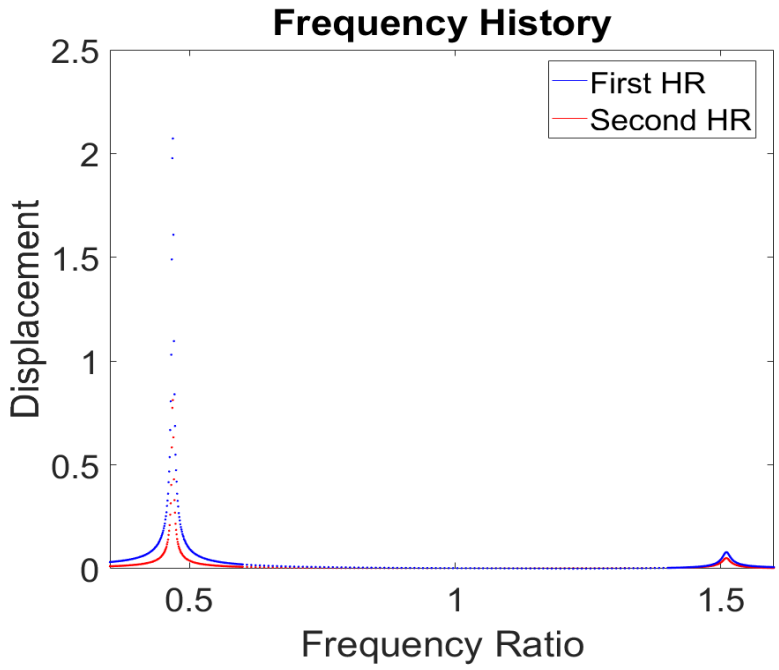

Figure 3.18: Frequency History for Dual HHR Analyzed Linearly (Second Case)

Time history at the first and second resonance frequencies are shown in figure 3.19 (a) and (b) respectively.

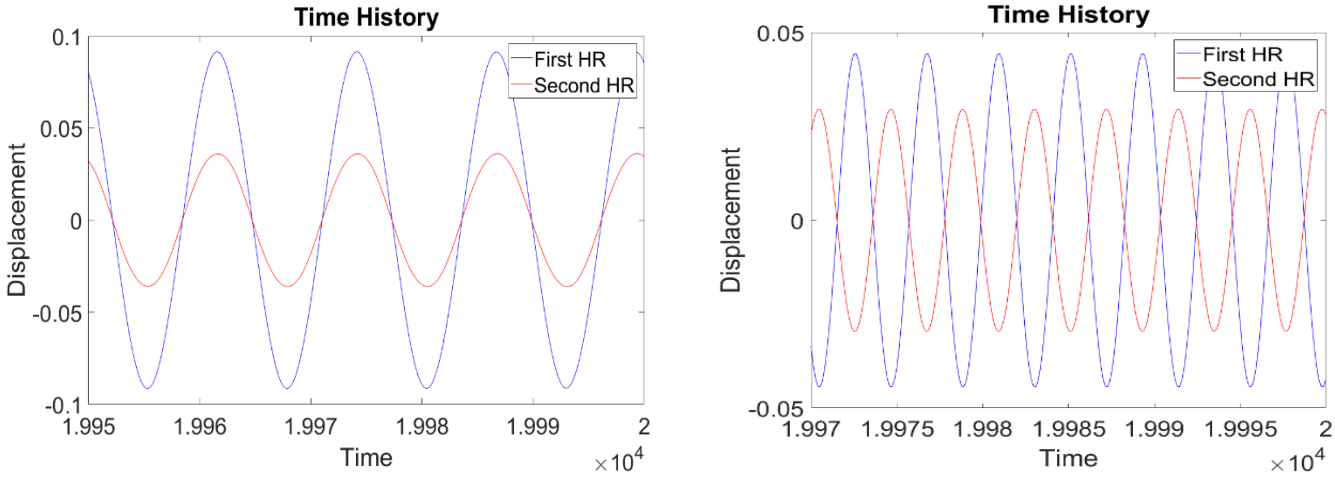

(a) **(b)**

Figure 3.19: Time History for Dual HHR Analyzed Linearly (Second Case) at (a) Frequency Ratio = 0.45 (b) Frequency Ratio = 1.55

CHAPTER 4

MATHEMATICAL ANALYSIS OF NONLINEAR HHR CONFIGURATIONS

4.1 Introduction

The HHRs discussed in chapter 3 are created to attenuate the sound pressure level under different configurations. However, air has a nonlinear behavior in terms of the thermodynamics process occurring inside the Helmholtz resonator [51]. As a result, in this chapter the nonlinearity is added to the governing equations of motion shown in sections 3.6 and 3.7 to explain the appearance of excess average pressure inside the resonator and a net reaction force acting on the resonator itself when the resonator is driven at high sound pressure levels such as in some applications where the waves with sufficiently high amplitudes are being dealt with by acousticians. Consequently, in such cases, nonlinear analysis has to be applied to justify the distortion of such a huge signal. In this chapter, the mathematical formulations of acoustic wave propagation in ducts with multiple configurations of HHRs are derived by applying nonlinear analysis. Each configuration response is generated using MATLAB, including checking for the chaos phenomenon. A comparison between the different configurations is also made, as well as comparing the obtained results with the linear analysis results.

In addition to the assumptions used in chapter 3, the following assumptions are also used for nonlinear analysis:

- Strictly forward wave propagation.
- Small Value of Viscosity.

Nonlinear Modeling for Different Configurations of Helmholtz Resonators

Four different configurations of HHRs are studied in detail in the following sections.

1. Nonlinear Modeling of a Single HHR installed to a two dimensional duct.
2. Nonlinear Modeling of a dual HHRs Connected in Series installed to a two dimensional duct.
3. Nonlinear Modeling of a Single HHR Connected in Series with Coupling Box and Kundt Tube.
4. Nonlinear Modeling of a Dual HHRs Connected in Series with a Coupling Box and Kundt Tube.

4.2 Nonlinear Analysis of a Single Helmholtz Resonator

Helmholtz resonators are usually used to attenuate a low range of frequencies (less than 1000 Hz). However, they are specific for a certain frequency to work on. Consequently, to overcome this limitation in the performance of the resonators, the nonlinearity in the stiffness and the damping terms are introduced here.

4.2.1 Governing Equation of Motion

The air inside the cavity is considered nonlinear in the low frequency domain, and its displacement in the tube produce a change in the pressure [31]:

$$\Delta p = -\rho_0 \mathrm{L}'_{c1} {\omega_0}^2 \left(x_{c1} - \frac{(\gamma+1)A_{c1}}{2V_1} x_{c1}^2 + \frac{(\gamma+1)(\gamma+2)A_{c1}^2}{6V_1^2} x_{c1}^3 \right) \tag{4.1}$$

The nonlinear damping force is due to jet phenomena. As a result, a nonlinear governing equation of motion for a single HHR with respect to time is obtained by adding the nonlinear terms to equation 3.15 as follows:

$$\begin{aligned} & m_1 \frac{d^2 x_{c1}}{\mathrm{d}t^2} + \frac{2m_1 A_{c1}}{2\rho_0 \mathrm{L}'_{c1}} R(Z_{in} + Z_{vis}) \left(\frac{dx_{c1}}{dt}\right) + \frac{\zeta m_1}{2\mathrm{L}'_{c1}} \left(\frac{dx_{c1}}{dt}\right)\left(\frac{dx_{c1}}{dt}\right) \\ & + \frac{\rho_0 c_0^2 A_{c1}}{V_1} \left(A_{c1} x_{c1} - \frac{(\gamma+1)A_{c1}^2}{2V_1} x_{c1}^2 + \frac{(\gamma+1)(\gamma+2)A_{c1}^3}{6V_1^2} x_{c1}^3 \right) = -p\mathrm{A}_{\mathrm{c1}} \end{aligned} \tag{4.2}$$

Introducing dimensionless variables, t*=$\omega_0 t$, $x = \frac{x_{c1}A_{c1}}{V_1}$, and assuming a harmonic excitation sound wave with forced frequency (ω), we get:

$$\frac{d^2x}{dt^{*2}} + c_1 \frac{dx}{dt^*} + c_3 \frac{dx}{dt^*}\left|\frac{dx}{dt^*}\right| + x + k_1 x^2 + k_2 x^3 = P\cos(\Omega t^*) \tag{4.3}$$

$$c_3 = \frac{\zeta V_1}{2\mathrm{L}'_{c1} A_{c1}}$$

$$k_1 = -\alpha = -\frac{(\gamma+1)}{2}$$

$$k_2 = \beta = \frac{(\gamma+1)(\gamma+2)}{6}$$

Table 4-1 shows the Helmholtz resonator's parameters which are used for the following obtained results:

Table 4-1: Physical Parameters for Single HHR with Nonlinear Parameters

No.	Parameters	HHR
1	Radius of the Neck	3.0 mm
2	Length of the Neck	9.0 mm
3	Radius of the Cavity	42.2 mm
4	Length of the Cavity	21.5 mm
5	Speed of Sound	340.0 m/s
6	Density of Air	1.2 kg/m^3
7	Specific Heat Ratio	1.4
8	Coefficient of Hydraulic Resistance	$2.1e^{-4}$
9	Linear Damping Coefficient	8.67 s^{-1}
10	Forced Frequency	(100~400) Hz
11	Incident Amplitude	(130~150) dB

4.2.2 Possibility of chaos

Since the governing equation of motion (4.3) contains both quadratic and cubic stiffness nonlinear terms, as well as a quadratic damping term, chaos may be possible in such a system.

A) Bifurcation Diagram

For the considered system the bifurcation diagram is obtained in figure 4.1. This figure shows that the motion of the system is periodic and a homoclinic orbit does not exist for

the applied sound pressure level (130~150) dB, which indicates that there is no possibility of chaos at this range.

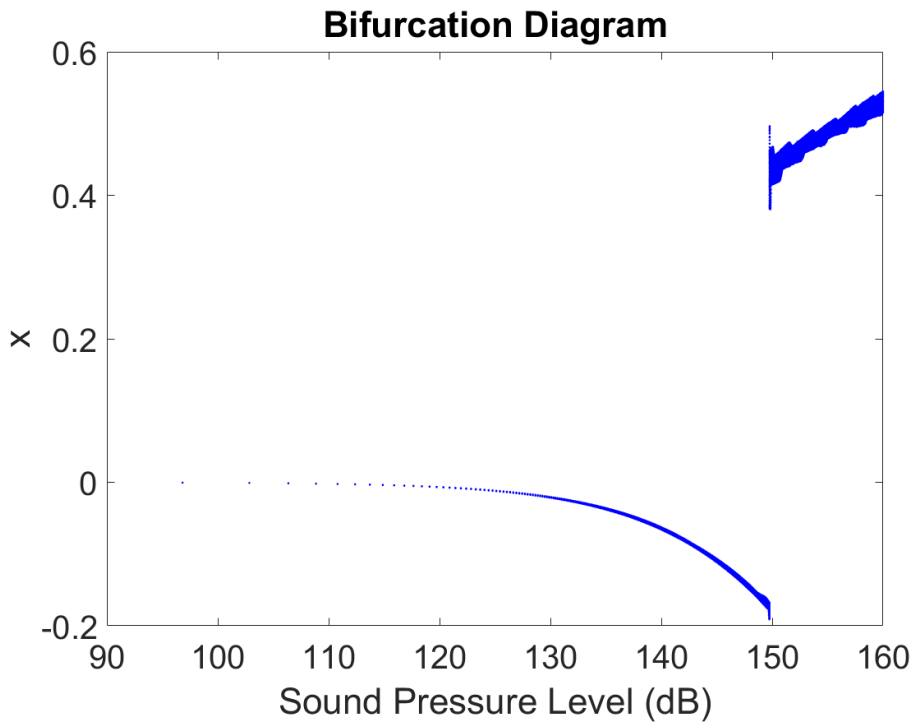

Figure 4.1: Bifurcation Diagram for Single HR Analyzed Nonlinearly with $\Omega = 1.01$

Comparing the obtained bifurcation diagram shown in the above figure with figure 3.7, which belongs to the linear system, we can observe the effect of the nonlinearity on the system behavior by setting the jump and discontinuity at 150 dB.

B) Phase Portraits

The relative Poincaré map for the system is shown for a sound pressure level of 150 dB. Figure 4.2 shows the quasiperiodic response of the system, which differs slightly from the purely periodic response of the linear system described in section 3.6.

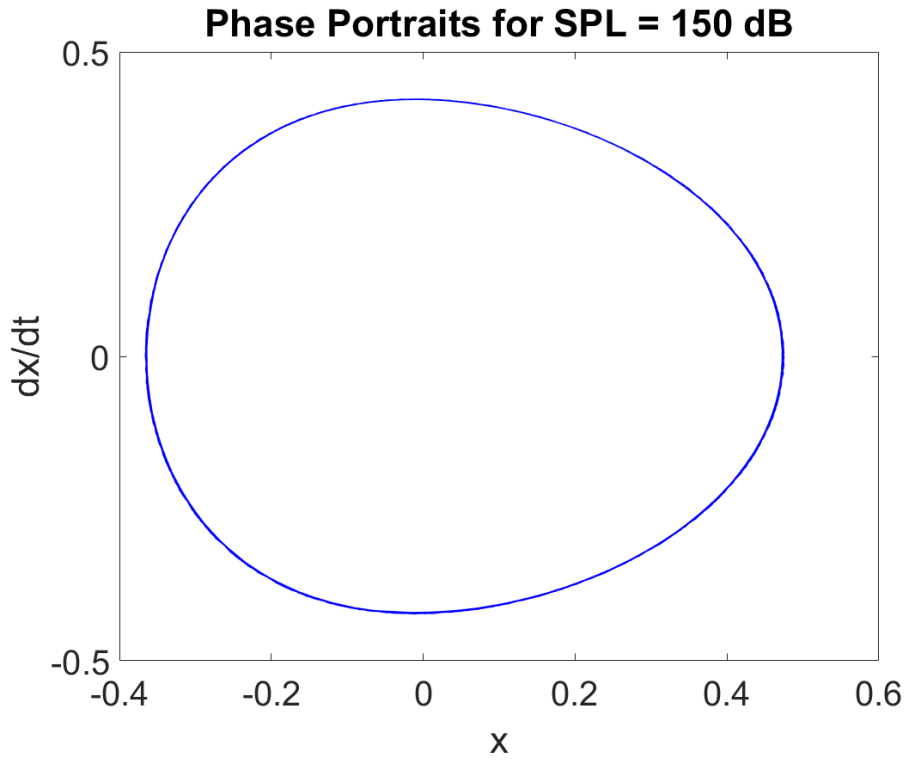

Figure 4.2: Phase Portraits for Single HHR Analyzed Nonlinearly Excited by 150 dB

4.2.3 Frequency and Time History

The numerical simulation of equation (4.3) presented in figure 4.3 shows an interesting behavior. That is for a low range of sound pressure level (130~140) dB, the system's resonance frequency is decreasing, while the amplitude is increasing, which is known as a

softening behavior. This behavior transforms into a hardening behavior for higher sound pressure levels (145 &150) dB. This unique behavior is unlike the frequency history for the linear system shown in figure 3.9, where the resonance frequencies occur only at $\Omega = 1.0$.

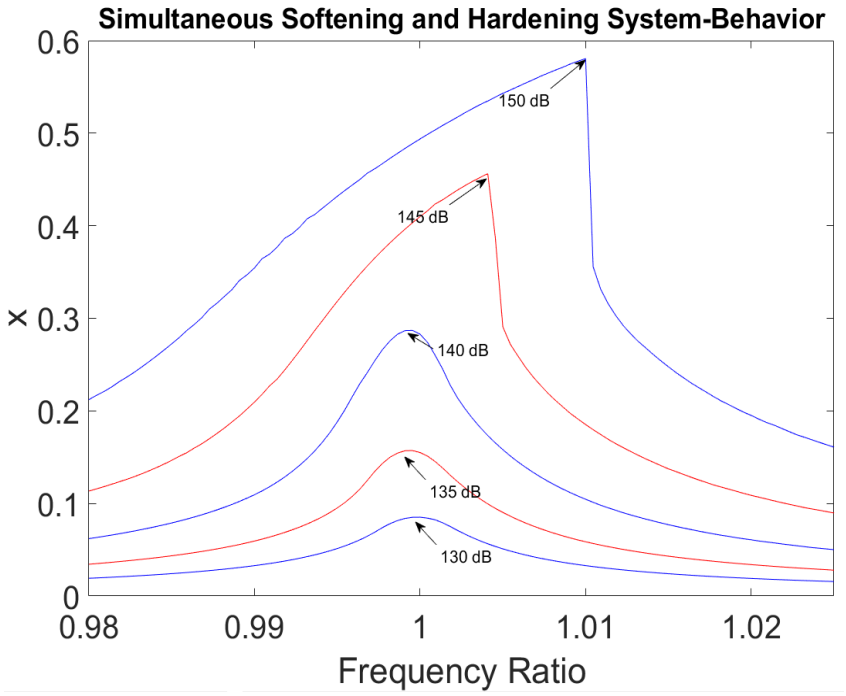

Figure 4.3: Simultaneous Softening and Hardening System Behavior for Dual HHR Analyzed Nonlinearly at Different SPL

Note that the nonlinear displacement shown in figure 4.3 does not exceed 0.6, while it reaches 0.8 in the linear analysis shown in figure 3.9, which justifies the appearance of excess average pressure inside the HHR due to vortex shedding at the outflow from the its opening.

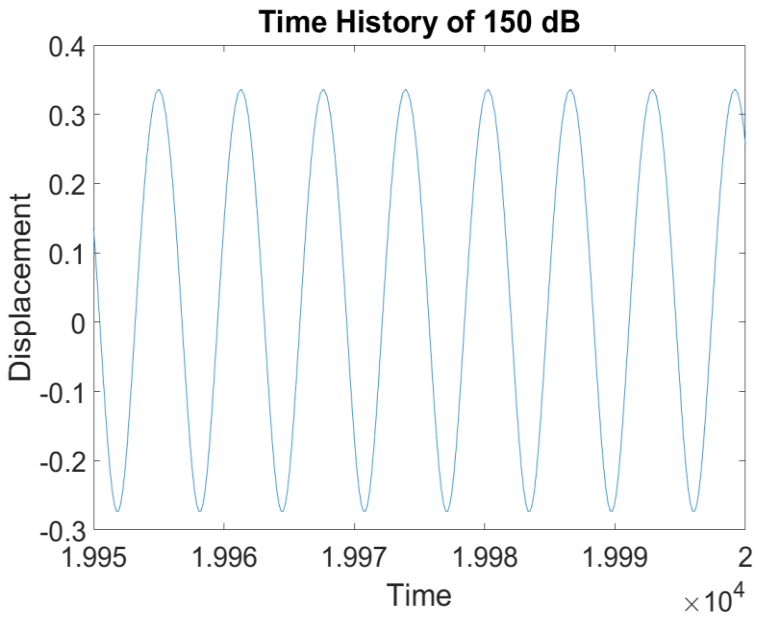

Figure 4.4: Time History for Dual HHR Analyzed Nonlinearly Excited by 150 dB

Harmonic behavior is detected for the sound pressure level of 150 dB as shown in figure 4.4, which is consistent with the frequency history.

4.3 Nonlinear Analysis of Dual Helmholtz Resonators

Nonlinear analysis for dual Helmholtz resonators enhances the accuracy of the response, especially if it is applied for both damping and stiffness terms at the same time. However, it has not been studied according to the best of my knowledge. As a result, in this section the governing equation of motion for a dual Helmholtz resonator under nonlinear analysis is derived, then the possibility of chaos is also studied before showing the amplitude response and whether the system has a softening or a hardening behavior. The results are compared to each other and with the desired linear systems described in section 3.7.

4.3.1 Governing Equation of Motion

The governing equations of motion for a nonlinear dual Helmholtz resonator system which appears in figure 4.5 are derived in the same way as the linear HHR in section 3.7, while the nonlinear terms of stiffness and damping, which have been explained in section 4.2, are added to the governing equations of motion.

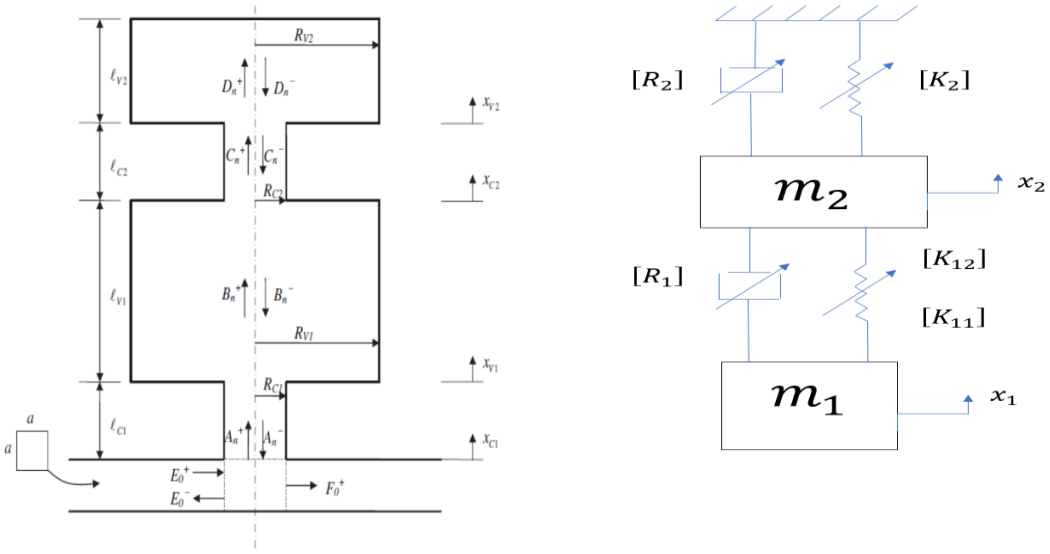

Figure 4.5: Dual Helmholtz Resonator with Nonlinear Parameters

The governing equation of motion for each HHR is derived using the rate of change of the momentum equation for each mass as shown below.

The nonlinear damping force is due to jet phenomena. As a result, nonlinear governing equations of motion for a dual HHR with respect to time are obtained by adding the nonlinear terms to equation 3.37 and 3.38 as follows:

$$
\begin{aligned}
&\mathrm{m}_1\frac{\mathrm{d}^2x_{c1}}{dt^2}+\frac{2\mathrm{m}_1A_{c1}}{2\rho_0\mathrm{L}'_{c1}}\left(\frac{dx_{c1}}{dt}-\frac{dx_{c2}}{dt}\right)+\frac{\zeta\mathrm{m}_1}{2\mathrm{L}'_{c1}}\left(\frac{dx_{c1}}{dt}\frac{dx_{c1}}{dt}-\frac{dx_{c2}}{dt}\frac{dx_{c2}}{dt}\right)\\
&+\frac{\rho_0c_0^2A_{c1}}{V_1}\left(A_{c1}x_{c1}-A_{c2}x_{c2}-\frac{(\gamma+1)}{2V_1}(A_{c1}^2x_{c1}^2-A_{c2}^2x_{c2}^2)\right.\\
&\left.+\frac{(\gamma+1)(\gamma+2)}{6V_1^2}(A_{c1}^3x_{c1}^3-A_{c2}^3x_{c2}^3)\right)=-p\mathrm{A}_{\mathrm{c1}}
\end{aligned}
\tag{4.4}
$$

$$
\begin{aligned}
&\mathrm{m}_2\frac{\mathrm{d}^2x_{c2}}{dt^2}+\frac{2m_1A_{c1}}{2\rho_0\mathrm{L}'_{c1}}R(Z_{in}+Z_{vis})\left(\frac{dx_{c2}}{dt}-\frac{dx_{c1}}{dt}\right)\\
&+\frac{\zeta\mathrm{m}_1}{2\mathrm{L}'_{c1}}\left(\frac{dx_{c2}}{dt}\frac{dx_{c2}}{dt}-\frac{dx_{c1}}{dt}\frac{dx_{c1}}{dt}\right)\\
&+\frac{\rho_0c_0^2A_{c2}}{V_1}\left(A_{c2}x_{c2}-A_{c1}x_{c1}-\frac{(\gamma+1)}{2V_1}(A_{c2}^2x_{c2}^2-A_{c1}^2x_{c1}^2)\right.\\
&\left.+\frac{(\gamma+1)(\gamma+2)}{6V_1^2}(A_{c2}^3x_{c2}^3-A_{c1}^3x_{c1}^3)\right)+\frac{2m_2A_{c2}}{2\rho_0\mathrm{L}'_{c2}}R(Z_{in}+Z_{vis})\left(\frac{dx_{c2}}{dt}\right)\\
&+\frac{\zeta m_2}{2\mathrm{L}'_{c2}}\left(\frac{dx_{c2}}{dt}\right)\left(\frac{dx_{c2}}{dt}\right)\\
&+\frac{\rho_0c_0^2A_{c2}^2}{V_2}\left(x_{c2}-\frac{(\gamma+1)A_{c2}}{2V_2}x_{c2}^2+\frac{(\gamma+1)(\gamma+2)A_{c2}^2}{6V_2^2}x_{c2}^3\right)=0
\end{aligned}
\tag{4.5}
$$

Similar to the approach applied in the previous sections, introducing dimensionless variables, t*=$\omega_{01}t$, $x_1=\frac{x_{c1}A_{c1}}{V_1}$, $x_2=\frac{x_{c2}A_{c2}}{V_2}$ and nonlinear damping coefficient $c_4=\frac{\zeta V_2}{2\mathrm{L}'_{c2}A_{c2}}$. Consequently, after assuming a harmonic excitation sound wave with forced frequency (ω), the dimensionless governing equations of motion are

$$\frac{d^2x_1}{\mathrm{d}t^{*2}} + c_1\left(\frac{dx_1}{dt^*} - \frac{A_{c1}V_2}{A_{c2}V_1}\frac{dx_2}{dt^*}\right) + c_3\left(\frac{dx_1}{dt^*}\left|\frac{dx_1}{dt^*}\right| - \frac{A_{c1}^2V_2^2}{A_{c2}^2V_1^2}\frac{dx_2}{dt^*}\left|\frac{dx_2}{dt^*}\right|\right)$$
$$+\left(x_1 - \frac{V_2}{V_1}x_2\right) + k_1\left(x_1^2 - \frac{V_2^2}{V_1^2}x_2^2\right) + k_2\left(x_1^3 - \frac{V_2^3}{V_1^3}x_2^3\right) = P\,cos(\Omega t^*) \quad (4.6)$$

$$\frac{d^2x_2}{\mathrm{d}t^{*2}} + r_1c_1\left(\frac{dx_2}{dt^*} - \frac{A_{c2}V_1}{A_{c1}V_2}\frac{dx_1}{dt^*}\right)$$
$$+ r_1c_3\frac{A_{c1}}{V_1}\left(\frac{V_2}{A_{c2}}\frac{dx_2}{dt^*}\left|\frac{dx_2}{dt^*}\right| - \frac{A_{c2}V_1^2}{A_{c1}^2V_2}\frac{dx_1}{dt^*}\left|\frac{dx_1}{dt^*}\right|\right)$$
$$+\frac{\mathrm{L}_{c1}'}{\mathrm{L}_{c2}'A_{c1}}\left(A_{c2}x_2 - \frac{A_{c2}V_1}{V_2}x_1\right) - \frac{\mathrm{L}_{c1}'\alpha}{\mathrm{L}_{c2}'A_{c1}V_1}\left(V_2A_{c2}x_2^2 - \frac{A_{c2}V_1^2}{V_2}x_1^2\right) \quad (4.7)$$
$$+\frac{\mathrm{L}_{c1}'\beta}{\mathrm{L}_{c2}'A_{c1}V_1^2}\left(A_{c2}V_2^2x_2^3 - \frac{A_{c2}V_1^3}{V_2}x_1^3\right) + c_2\frac{dx_2}{dt^*} + c_4\frac{dx_2}{dt^*}\left|\frac{dx_2}{dt^*}\right| + r_2^2x_2$$
$$-\alpha r_2^2x_2^2 + \beta r_2^2x_2^3 = 0$$

Table 4-2: Physical Parameters for Dual HHR with Nonlinear Parameters

No.	Parameters	First HHR	Second HHR
1	Radius of the Neck	3.0 mm	3.0 mm
2	Length of the Neck	9.0 mm	9.0 mm
3	Radius of the Cavity	42.2 mm	42.2 mm
4	Length of the Cavity	21.5 mm	21.5 mm
5	Linear Damping Coefficient	8.67 s^{-1}	8.67 s^{-1}
6	Speed of Sound	340.0 m/s	
7	Density of Air	1.2 kg/m^3	
8	Specific Heat Ratio	1.4	
9	Coefficient of Hydraulic Resistance	2.1e^{-4}	
10	Forced Frequency	(100~400) Hz	
11	Incident Amplitude	(130~150) dB	

Table 4-2 shows the Helmholtz resonators' parameters which are used for the following obtained results:

4.3.2 Possibility of chaos

The main concern of this section is tracing the bifurcation diagram and identifying the periodic motions and the chaotic motion.

A) Bifurcation Diagram

Figure 4.6 shows that the motion of the system is periodic and the homoclinic orbit does not exist for the applied sound pressure level (130~150) dB, which indicates that there is no possibility of chaos at this range.

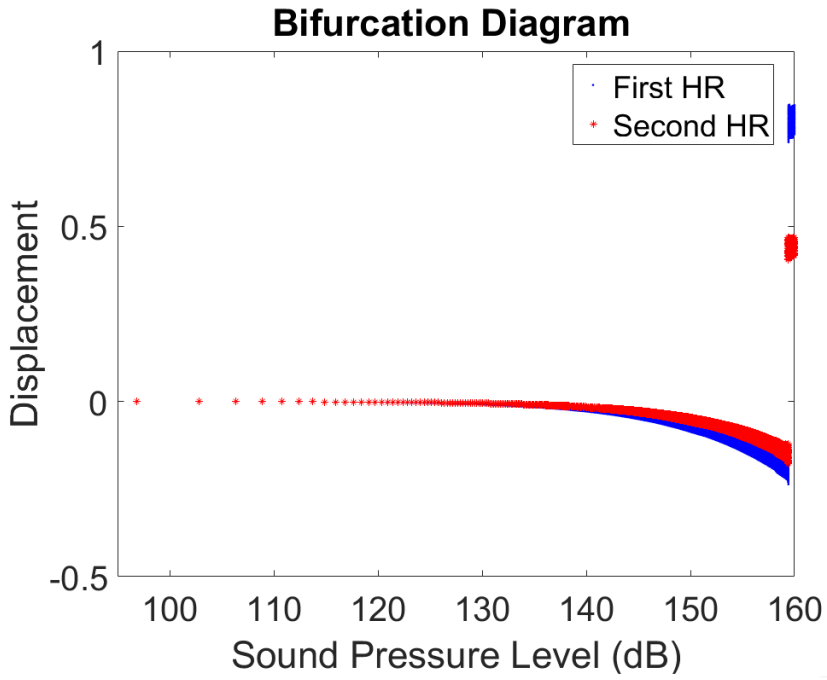

Figure 4.6: Bifurcation Diagram for Dual HHR Analyzed Nonlinearly with $\Omega = 1.01$

Comparing the obtained bifurcation diagram shown in the above figure with figure 3.14, which belongs to the linear dual HHR system, we can observe the effect of nonlinearity on the system behavior by setting the jump and discontinuity at high sound pressure levels, which leads to instability in the solution. However, this is not located in our targeted range of sound pressure levels (130~150) dB.

B) Phase Portraits

In this section, the relative phase portraits for the dual Helmholtz resonator system are studied at 150 dB. Figure 4.7 describes the quasiperiodic motion for the applied sound pressure level (150 dB).

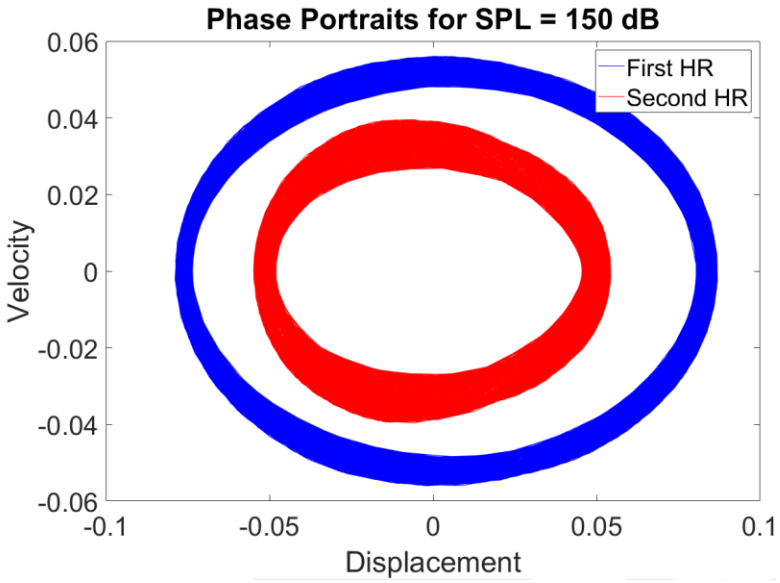

Figure 4.7: Phase Portraits for Quasiperiodic Dual HHR Analyzed Nonlinearly Excited by SPL = 150 dB

Note that the motion moved from a purely periodic behavior in the linear dual HHR system shown in figure 3.15, to a quasiperiodic motion in the nonlinear system shown above.

4.3.3 Frequency and Time History

Numerical simulations of equations (4.6) and (4.7) are simulated for two different cases to examine the effect of the HHRs dimensions on the resonance frequency, as well as the displacement, the two different cases are:

1. Identical Masses and Volumes for both Helmholtz Resonators.
2. Identical Masses for both Helmholtz Resonators, While the Volume of the Second HHR-Cavity is double the Volume of the First HHR-Cavity.

For the case of identical dimensions for both HHRs, the frequency history is shown in figure 4.8, where the first and second resonance frequencies occur at the same range of the linear frequency ratio (i.e. 0.65 and 1.65, respectively). However, the hardening behavior is clearly observed in the nonlinear response at the first resonance frequency. Also, the magnitude of displacement reaches only 0.68 at the first resonance frequency. However, it exceeds 2.5 at the linear system for the same range of frequency ratio (0.65). Due to the effect of the vortex shedding at the inlet of the HHR. On the other hand, the magnitude of the second HHR displacement at the second resonance frequency is larger than the first HHR one, which is consistent with the result obtained from figure 3.16 in the linear system.

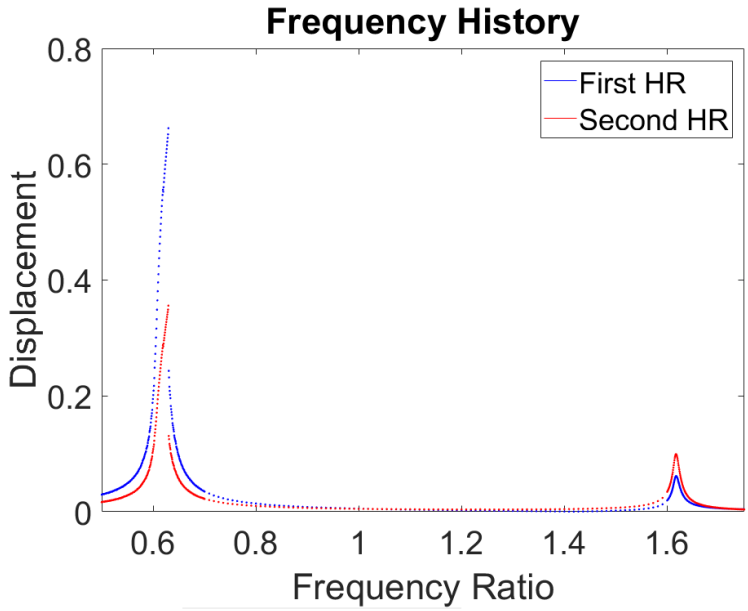

Figure 4.8: Frequency History for Dual HHR Analyzed Nonlinearly (First Case)

Time history at the both resonance frequencies are shown in figures 4.9 (a) and (b).

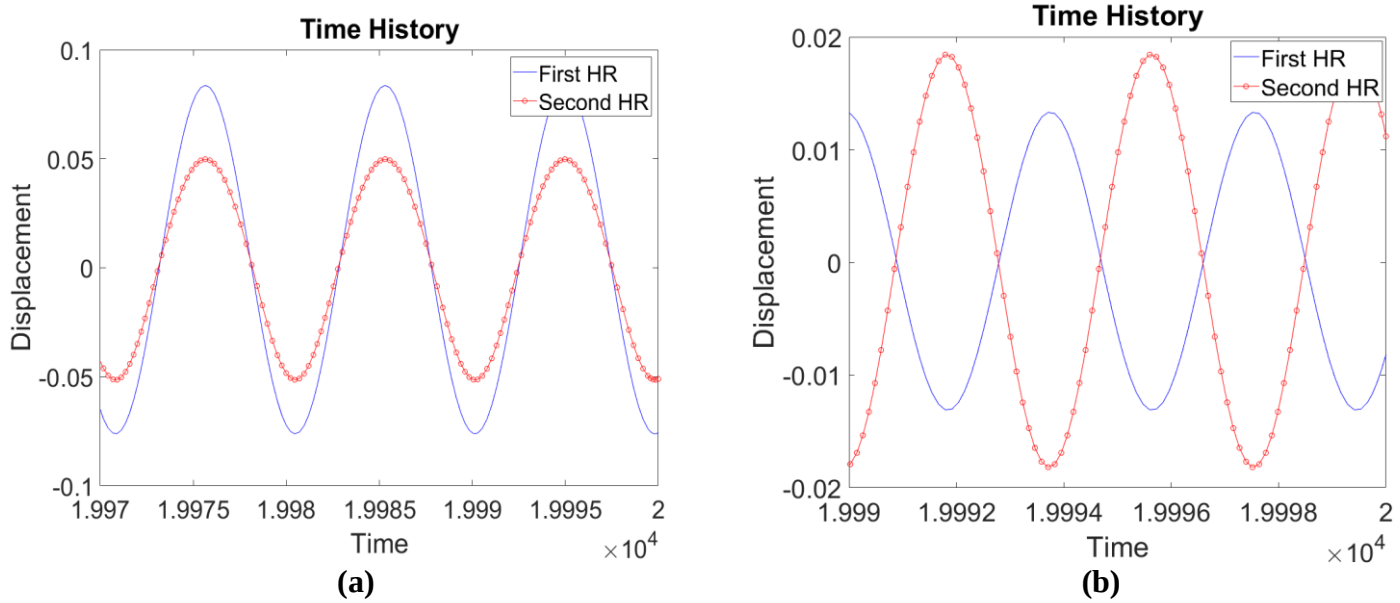

Figure 4.9: Time History for Dual HHR Analyzed Nonlinearly (First Case) at

(a) Frequency Ratio = 0.65 (b) Frequency Ratio = 1.6

For the second case where ($m_1=m_2$ and $V_2= 2V_1$), the frequency history is shown in figure 4.10, where the first and second resonance frequencies occur at smaller frequency ratios (0.45 and 1.55), respectively.

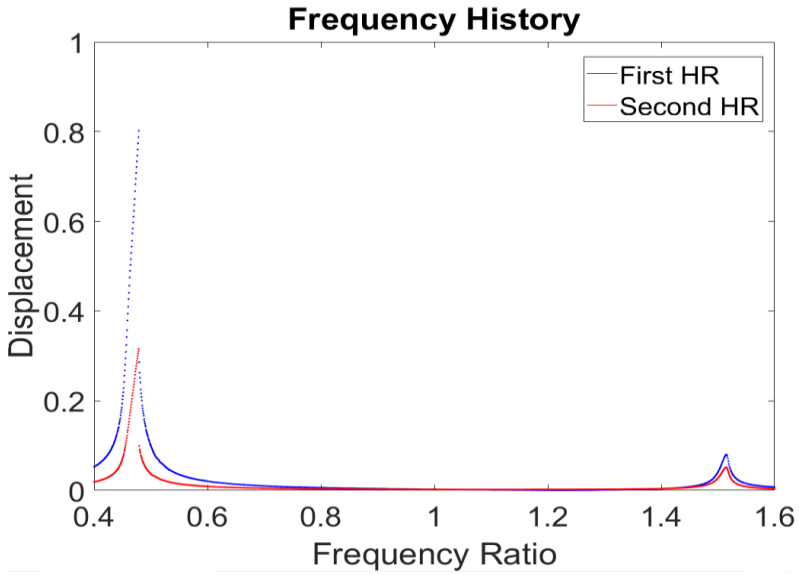

Figure 4.10: Frequency History for Dual HHR Analyzed Nonlinearly (Second Case)

The magnitude of displacement reaches 0.80 at the first resonance frequency. However, it does not exceed 0.70 in the first case. Also, contrary to the first case, the magnitude of the first HHR displacement at the second resonance frequency is larger than the second HHR one. Comparing the small displacement shown in figure 4.10, with respect to the one obtained using linear analysis for the same case shown in figure 3.18, we can justify the appearance of excess average pressure inside the resonator and a net reaction force acting on the resonator itself when the resonator is driven at high sound pressure levels such as 150 dB.

Time history at the two resonance frequencies are shown in figures 4.11 (a) and (b).

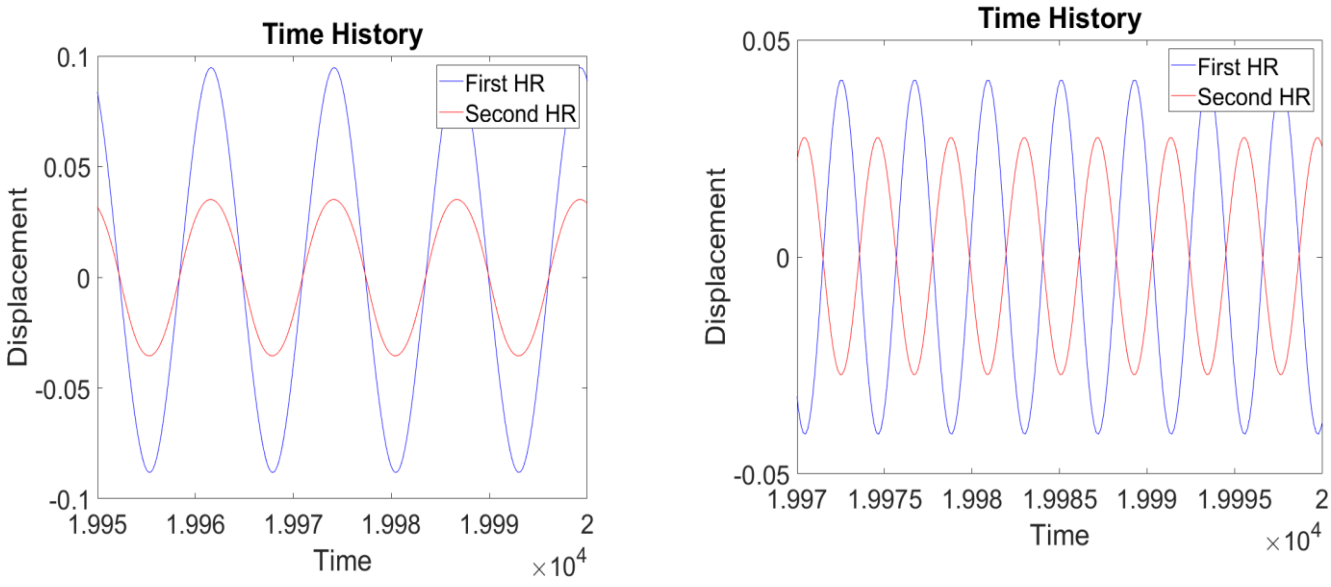

(a) **(b)**

Figure 4.11: Time History for Dual HHR Analyzed Nonlinearly (Second Case) at (a) Frequency Ratio = 0.45 (b) Frequency Ratio = 1.55

4.4 Nonlinear Modeling of a Single HHR Connected in Series with Coupling Box and Kundt Tube

A Kundt's tube is an old invention that was used in the 19th century to measure the speed of sound inside air or a solid medium. It consists of a horizontal pipe that contains a soft powder. One of its ends relates to a loudspeaker, while the other end is attached to a Helmholtz resonator. A signal's wavelength is identified using the Kundt's tube by applying a source of energy and tuning it until the tube starts vibrating. The wavelength is calculated based on the tube's length, which is used to calculate the resonance frequency [32]. Nowadays it is being used for analyzing standing waves and acoustical forces. In

this section, a single HHR is connected to a Kundt tube and a coupling box, as appears in figure 4.12.

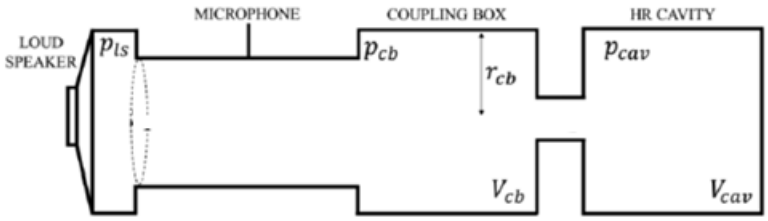

Figure 4.12: Single HHR Coupled with Kundt Tube Using a Coupling Box

The governing equation of motion for each component is derived before getting a response using MATLAB.

4.4.1 Governing Equation of Motion

In order to obtain the governing equation of motion for the coupled system, the governing equation of each part is considered.

Starting from the Kundt tube by applying the conservation of mass and considering a single degree of freedom there (1 DOF), we can write

$$\frac{\partial \rho_0}{\partial t} + \rho_0 div(\frac{\partial x_t}{\partial t}) = 0 \tag{4.8}$$

The equation of the fluid in the linear domain is written as

$$\frac{\partial p}{\partial \rho_0} = c_0^2 \tag{4.9}$$

By substituting equation 4.9 into equation 4.8, we obtain

$$\frac{1}{c_0^2}\frac{\partial p}{\partial t} + \rho_0 \frac{\partial}{\partial X}\left(\frac{\partial x_t}{\partial t}\right) = 0 \tag{4.10}$$

Where X is the space variable. Equation 4.10 reads as

$$\frac{\partial p}{\partial t} = -\rho_0 c_0^2 \frac{\partial}{\partial X}\left(\frac{\partial x_t}{\partial t}\right) \tag{4.11}$$

So,

$$p = -\rho_0 c_0^2 \frac{\partial x_t}{\partial X} \tag{4.12}$$

Euler's equation for planar wave is considered.

$$\rho_0 \frac{\partial^2 x_t}{\partial t^2} = \frac{\partial}{\partial X}\left(\rho_0 c_0^2 \frac{\partial x_t}{\partial X}\right) \tag{4.13}$$

By integrating equation 4.13 along the tube's length and using the Rayleigh-Ritz method, while applying the forces at the tube's boundaries and considering a dapping term, the governing equation of motion for the tube reads as

$$m_t \frac{d^2 x_t}{\mathrm{d}t^2} + c_t \frac{dx_t}{dt} + k_t x_t = p_{ls} S_t - p_{cb} S_t \tag{4.14}$$

Where p_{ls} is the loudspeaker's pressure, $p_{cb}$is the pressure of the coupling box.

$$m_t = \rho S_t L_{et}/2 \tag{4.15}$$

$$S_t = r_t^2 \pi \tag{4.16}$$

Where L_{et} and r_t are the tube's effective length and radius respectively.

$$k_t = \rho_0 S_t c_0^2 \pi^2 / 2 L_{et} \tag{4.17}$$

$$p_{cb} = \frac{-\rho_0 c_0^2}{V_{cb}}(S_1 x_{c1} - S_t x_t) \tag{4.18}$$

$$V_{cb} = r_{cb}^2 \pi L_{cb} \tag{4.19}$$

$$p_{ls} = P\cos(\omega_f t) \tag{4.20}$$

Where $L_{cb}\ and\ \omega_f$ are the length of the coupling box and forcing angular frequency respectively.

So, after substituting the whole terms the governing equation of motion for the Kundt tube reads as:

$$m_t \frac{d^2 x_t}{\mathrm{d}t^2} + c_t \frac{dx_t}{dt} + \frac{\rho S_t c_0^2 \pi^2}{2L_{et}} x_t - \frac{\rho c_0^2}{V_{cb}}(S_1 x_{c1} - S_t x_t) = P\cos(\omega_f t) \tag{4.21}$$

Secondly, based on the derived equation for a single HHR in section 4.2, the nonlinear governing equation of motion for the HHR coupled with Kundt tube after inserting the coupling term reads as

$$\begin{aligned} &m_1 \frac{d^2 x_{c1}}{dt^2} + \frac{S_1 m_1}{\rho L_{e1}} R(Z_{in} + Z_{vis}) \frac{dx_{c1}}{dt} + \frac{\zeta m_1}{2L_{e1}} \frac{dx_{c1}}{dt}\left|\frac{dx_{c1}}{dt}\right| + \rho S_1 L_{e1} \omega_{01}^2 x_{c1} \\ &- \rho L_{e1} \omega_{01}^2 \frac{\alpha S_1^2}{V_1} x_{c1}^2 + \rho L_{e1} \omega_{01}^2 \frac{\beta S_1^3}{{V_1}^2} x_{c1}^3 + \frac{\rho c_0^2}{V_{cb}}(S_1 x_{c1} - S_t x_t) = 0 \end{aligned} \tag{4.22}$$

Introducing normalized time, t*=$\omega_t t$, where $\omega_t = \sqrt{k_t/m_t}$. By denoting $k_{t1} = \rho c_0^2 S_1 S_t / V_{cb}$ and $\omega_n = \omega/\omega_t$, we have

$$\frac{d^2x_t}{\mathrm{d}t^{*2}} + \frac{c_t}{\sqrt{k_t m_t}}\frac{dx_t}{dt^*} + x_t - \frac{k_{t1}}{k_t}\left(x_{c1} - \frac{S_t}{S_1}x_t\right) = \frac{P}{k_t}\cos(\omega_n t^*)$$

$$\frac{m_1}{m_t}\frac{d^2x_{c1}}{dt^{*2}} + \frac{S_1 m_1}{\sqrt{k_t m_t}\,\rho L_{e1}}R(Z_{in} + Z_{vis})\frac{dx_{c1}}{dt^*} + \frac{\zeta m_1}{2L_{e1}m_t}\frac{dx_{c1}}{dt^*}\left|\frac{dx_{c1}}{dt^*}\right| \qquad (4.23)$$

$$+ \frac{\rho S_1 L_{e1}\omega_{01}^2}{k_t}\left(x_{c1} - \frac{\alpha S_1}{V_1}x_{c1}^2 + \frac{\beta S_1^2}{{V_1}^2}x_{c1}^3\right) + \frac{k_{t1}}{k_t}\left(\frac{S_1}{S_t}x_{c1} - x_t\right) = 0$$

4.4.2 System Response

Table 4-3 describes the physical dimensions and parameters for the Single HHR system coupled with a Kundt Tube in series, which are used in the following sections.

Table 4-3: Physical Parameters for Single HHR Coupled with Kundt Tube

No.	Parameters	Kundt Tube and Coupling Box	HHR
1	Radius of the Neck	14.50 mm	3.0 mm
2	Length of the Neck	400.0 mm	9.0 mm
3	Radius of the Cavity	23.0 mm	42.2 mm
4	Length of the Cavity	232.5 mm	21.5 mm
5	Linear Damping Coefficient	0.025 $Kg.s^{-1}$	8.67 s^{-1}
6	Coefficient of Hydraulic Resistance	-	$2.1e^{-4}$
7	Forced Frequency	450 Hz	
8	Incident Amplitude	150 dB	
9	Speed of Sound	340.0 m/s	
10	Density of Air	1.20 kg/m^3	
11	Specific Heat Ratio	1.40	

Steady state and transient solutions are used to describe the displacement at the middle of the Kundt tube after applying a continuous sound pressure level and free response respectively. System's response is examined under both cases as well as the frequency and time history are obtained in the followings.

A) Steady State Response

A sinusoidal signal is sent to the small tube with a frequency of 450 Hz to excite the acoustical mode in the dynamic regime. Then we record the decreasing evolution of the response for two configurations: the tube with and without a coupled HR, and for levels of incident amplitude 150 dB.

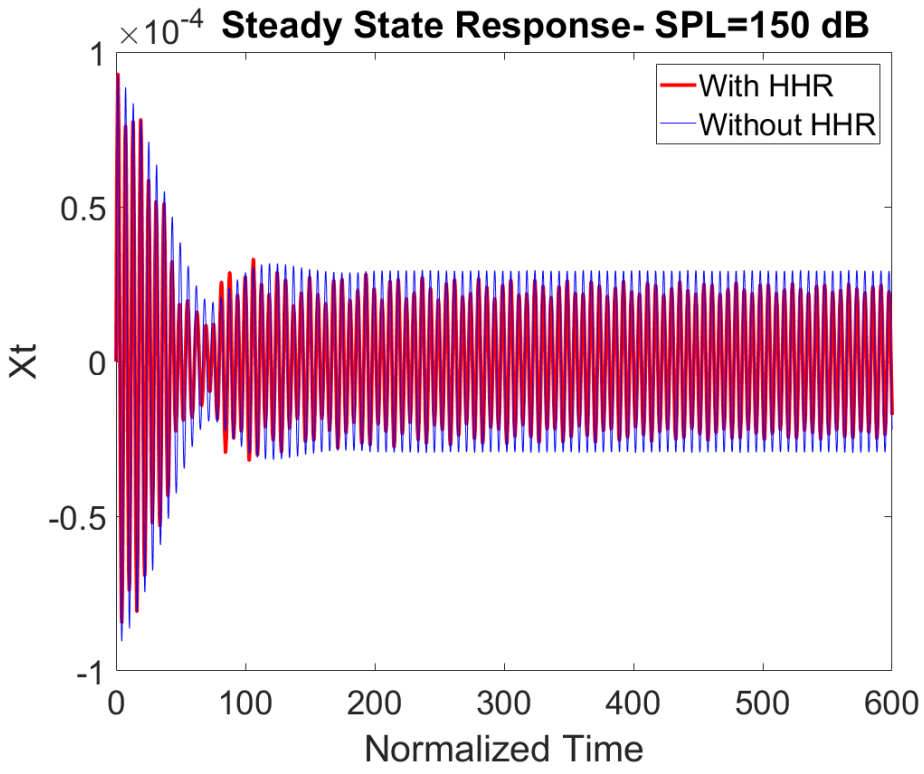

Figure 4.13: Steady State Response of Single HHR Connected with Kundt Tube

From figure 4.13 we can see that the absorption of the energy is better in the case with the coupled HHR as the displacement in the middle of the Kundt tube is smaller. In fact, coupling an HHR allows for absorbtion of energy in a faster manner, compared to the system without an HHR.

B) Transient Response

In order to simulate the free vibrations regime, we send a sinusoidal signal to the small tube with the frequency 450 Hz to excite the acoustical mode in the stationary regime. Then we stop the signal and we record the decreasing evolution of the response shown in figure 4.14, for two configurations: the tube with and without a coupled HR, and for levels of incident amplitude 150 dB.

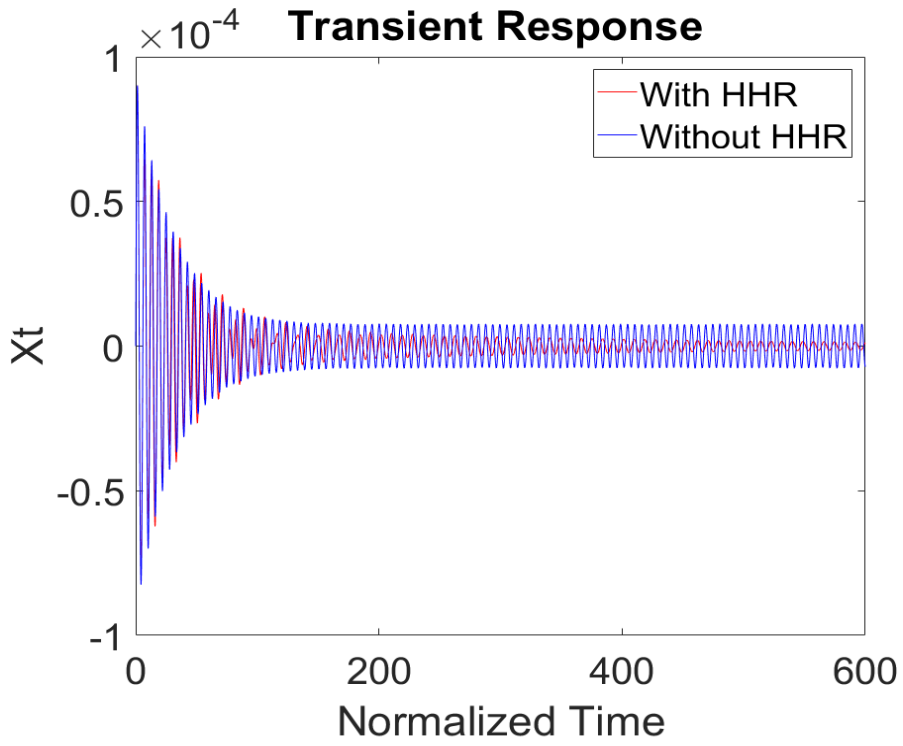

Figure 4.14: Transient Response of Single HHR Connected with Kundt Tube

Similar to the result obtained in the steady state solution, we can see that the absorption of the energy is better for the case with the coupled HHR as the displacement in the middle of the Kundt tube is smaller. This scenario is typical behavior for a targeted energy transfer and has already been underlined by Cochelin et al. [49].

C) Frequency History

In order to simulate the stationary response, a sweep sinusoidal signal is sent to study the behavior of a system as a function of frequency. The results are shown in Figure 4.15. Contrary to a linear absorber where two peaks appear, the curve with coupling a nonlinear resonator stays below the curve without a coupled HR.

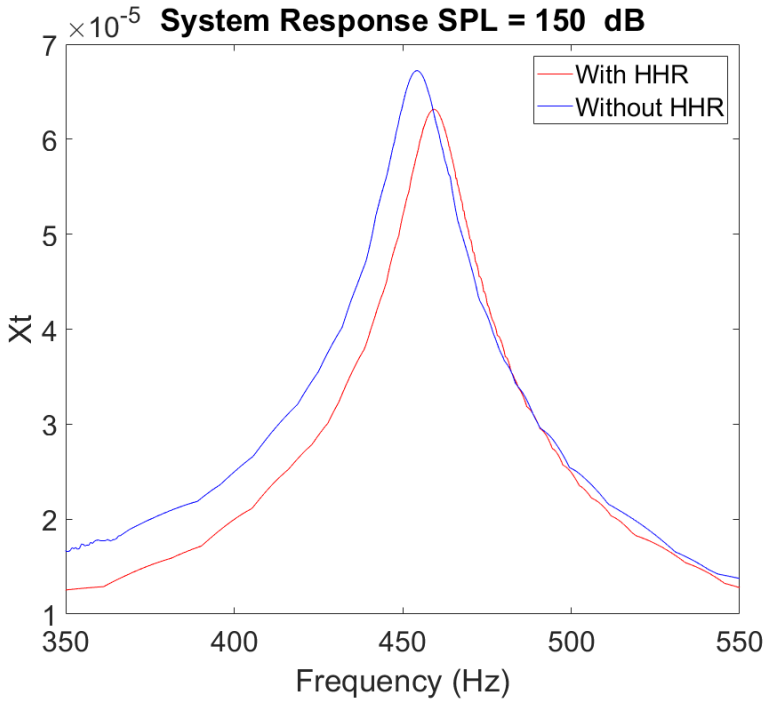

Figure 4.15: Frequency History for Single HHR Coupled with Kundt Tube

As a result, the nonlinear HR is efficient, not only for a single frequency, but also for a larger band of frequencies. However, for the stationary regime, we did not succeed in

activating quasi periodic behavior for some frequency bands. Also, a phase shift in the resonance frequency is produced because of the coupled HHR.

D) Time Hisotry

A periodic response is illustrated from the time history shown in figure 4.16. Pressure amplitude at the middle of the Kundt tube is also smaller in the case of the coupled HHR, which is consistent with the preceding results.

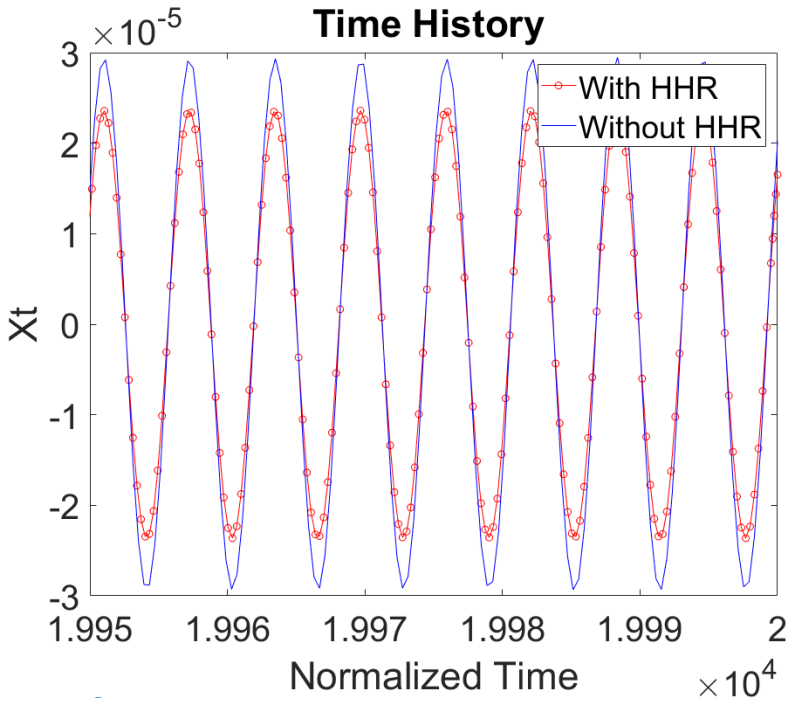

Figure 4.16: Time History for Single HHR Coupled with Kundt Tube

4.5 Nonlinear Modeling of a Dual HHRs Connected in Series with Coupling Box and Kundt Tube

Connecting a dual HHR with a Kundt tube in series, similar to figure 4.17, can improve the performance of the dual HHR described in section 4.4. There are three coupled equations and three resonance frequencies instead of two. This unique system has not been studied in the area of acoustics yet.

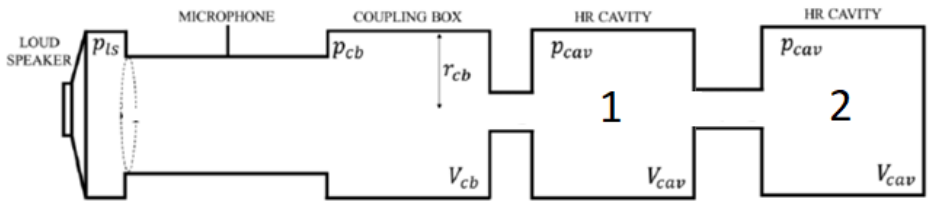

Figure 4.17: Dual HHR Connected with Kundt Tube and Coupling Box in Series

4.5.1 Governing Equation of Motion for the System

The governing equation of motion for the Kundt tube is the same as per equation (4.21) in section 4.4. While the derived governing equation of motion for the first HHR (4.22) in the same section has an additional term because of the coupling with the second HHR. Consequently, the governing equation of motion of the first HHR is:

$$m_1\frac{d^2x_{c1}}{dt^2}+\frac{S_1m_1}{\rho L_{e1}}R(Z_{in}+Z_{vis})\left(\frac{dx_{c1}}{dt}-\frac{dx_{c2}}{dt}\right)$$

$$+\frac{\zeta m_1}{2L_{e1}}\left(\frac{dx_{c1}}{dt}\left|\frac{dx_{c1}}{dt}\right|-\frac{dx_{c2}}{dt}\left|\frac{dx_{c2}}{dt}\right|\right)+\rho L_{e1}\omega_{01}^2(S_1x_{c1}-S_2x_{c2})$$

$$-\rho L_{e1}\omega_{01}^2\frac{\alpha}{V_1}(S_1^2x_{c1}^2-S_2^2x_{c2}^2)+\rho L_{e1}\omega_{01}^2\frac{\beta}{{V_1}^2}(S_1^3x_{c1}^3-S_2^3x_{c2}^3) \quad (4.24)$$

$$+\frac{\rho c_0^2}{V_{cb}}(S_1x_{c1}-S_tx_t)=0$$

Where $x_{c2}\ and\ S_2$ describes the motion and neck area of the second HHR, respectively.

Similarly, the governing equation of motion for the second HHR is

$$\mathrm{m}_2\frac{\mathrm{d}^2x_{c2}}{dt^2}+\frac{2m_1S_1}{2\rho_0L_{e1}}R(Z_{in}+Z_{vis})\left(\frac{dx_{c2}}{dt}-\frac{dx_{c1}}{dt}\right)$$

$$+\frac{\zeta\mathrm{m}_1}{2L_{e1}}\left(\frac{dx_{c2}}{dt}\frac{dx_{c2}}{dt}-\frac{dx_{c1}}{dt}\frac{dx_{c1}}{dt}\right)$$

$$+\frac{\rho L_{e1}\omega_{01}^2S_2}{S_1}\left(S_2x_{c2}-S_1x_{c1}-\frac{\alpha}{V_1}(S_2^2x_{c2}^2-S_1^2x_{c1}^2)+\frac{\beta}{{V_1}^2}(S_2^3x_{c2}^3-S_1^3x_{c1}^3)\right) \quad (4.25)$$

$$+\frac{2m_2S_2}{2\rho_0L_{e2}}R(Z_{in}+Z_{vis})\left(\frac{dx_{c2}}{dt}\right)+\frac{\zeta m_2}{2L_{e2}}\left(\frac{dx_{c2}}{dt}\right)\left(\frac{dx_{c2}}{dt}\right)$$

$$+\rho L_{e2}\omega_{02}^2\left(S_2x_{c2}-\frac{\alpha}{V_2}S_2^2x_{c2}^2+\frac{\beta}{{V_2}^2}S_2^3x_{c2}^3\right)=0$$

Similar to the procedure used in section 4.4, by introducing normalized time, t*=$\omega_t t$, where $\omega_t=\sqrt{k_t/m_t}$ By denoting $k_{t1}=\rho c_0^2S_1S_t/V_{cb}$ and $\omega_n=\omega/\omega_t$, we have

$$\frac{d^2x_t}{\mathrm{d}t^{*2}} + \frac{c_t}{\sqrt{k_t m_t}}\frac{dx_t}{dt^*} + x_t - \frac{k_{t1}}{k_t}\left(x_{c1} - \frac{S_t}{S_1}x_t\right) = \frac{P}{k_t}\cos(\omega_n t^*)$$

$$\frac{m_1}{m_t}\frac{d^2x_{c1}}{dt^{*2}} + \frac{S_1 m_1}{\sqrt{k_t m_t}\,\rho L_{e1}}R(Z_{in}+Z_{vis})\left(\frac{dx_{c1}}{dt^*} - \frac{dx_{c2}}{dt^*}\right)$$

$$+ \frac{\zeta m_1}{2L_{e1}m_t}\left(\frac{dx_{c1}}{dt^*}\left|\frac{dx_{c1}}{dt^*}\right| - \frac{dx_{c2}}{dt^*}\left|\frac{dx_{c2}}{dt^*}\right|\right) + \frac{\rho L_{e1}\omega_{01}^2}{k_t}(S_1 x_{c1} - S_2 x_{c2})$$

$$- \frac{\alpha\rho L_{e1}\omega_{01}^2}{V_1 k_t}(S_1^2 x_{c1}^2 - S_2^2 x_{c2}^2) + \frac{\beta\rho L_{e1}\omega_{01}^2}{{V_1}^2 k_t}(S_1^3 x_{c1}^3 - S_2^3 x_{c2}^3)$$

$$+ \frac{k_{t1}}{k_t}\left(\frac{S_1}{S_t}x_{c1} - x_t\right) = 0$$

$$\frac{m_2}{m_t}\frac{d^2x_{c2}}{dt^{*2}} + \frac{S_1 m_1}{\sqrt{k_t m_t}\,\rho L_{e1}}R(Z_{in}+Z_{vis})\left(\frac{dx_{c2}}{dt^*} - \frac{dx_{c2}}{dt^*}\right) \tag{4.26}$$

$$+ \frac{\zeta m_1}{2L_{e1}m_t}\left(\frac{dx_{c2}}{dt^*}\left|\frac{dx_{c2}}{dt^*}\right| - \frac{dx_{c2}}{dt^*}\left|\frac{dx_{c2}}{dt^*}\right|\right) + \frac{\rho L_{e1}\omega_{01}^2 S_2}{k_t S_1}(S_2 x_{c2} - S_1 x_{c1})$$

$$- \frac{\alpha\rho L_{e1}\omega_{01}^2 S_2}{V_1 k_t S_1}(S_2^2 x_{c2}^2 - S_1^2 x_{c1}^2) + \frac{\beta\rho L_{e1}\omega_{01}^2 S_2}{{V_1}^2 k_t S_1}(S_2^3 x_{c2}^3 - S_1^3 x_{c1}^3)$$

$$+ \frac{S_2 m_2}{\sqrt{k_t m_t}\,\rho L_{e2}}R(Z_{in}+Z_{vis})\frac{dx_{c2}}{dt^*} + \frac{\zeta m_2}{2L_{e2}m_t}\frac{dx_{c2}}{dt^*}\left|\frac{dx_{c2}}{dt^*}\right|$$

$$+ \frac{\rho S_2 L_{e2}\omega_{02}^2}{k_t}\left(x_{c2} - \frac{\alpha S_2}{V_2}x_{c2}^2 + \frac{\beta S_2^2}{{V_2}^2}x_{c2}^3\right) = 0$$

4.5.2 System Response

Table 4-4 shows the physical parameters and the parameters for the Dual HHR system coupled with a Kundt tube, which are used in the following sections.

Table 4-4: Physical Parameters for Dual HHR Coupled with Kundt Tube

No.	Parameters	Kundt Tube and Coupling Box	First HHR	Second HHR
1	Radius of the Neck	14.50 mm	3.0 mm	1.5 mm
2	Length of the Neck	400.0 mm	9.0 mm	4.5 mm
3	Radius of the Cavity	23.0 mm	42.2 mm	84.4 mm
4	Length of the Cavity	232.5 mm	21.5 mm	43.0 mm
5	Linear Damping Coefficient	0.025 $Kg.s^{-1}$	8.67 s^{-1}	4.34 s^{-1}
6	Coefficient of Hydraulic Resistance	-	$2.1e^{-4}$	
7	Forced Frequency	450 Hz	1.87	
8	Incident Amplitude	150 dB		
9	Speed of Sound	340.0 m/s		
10	Density of Air	1.20 kg/m^3		
11	Specific Heat Ratio	1.40		

Steady state and transient solutions are used to describe the displacement at the middle of the Kundt tube after applying a continuous sound pressure level and free response respectively. Similar to section 4.4, system's response under both cases as well as the frequency and time history are conducted below.

A) Steady State Response

A sinusoidal signal is sent to the small tube with a frequency 450 Hz to excite the acoustical mode in the dynamic regime. Then, the decreasing evolutions of the response for three configurations are recorded: the tube with a dual HHR, with a single HHR and without coupled HHRs, and for levels of incident amplitude 150 dB.

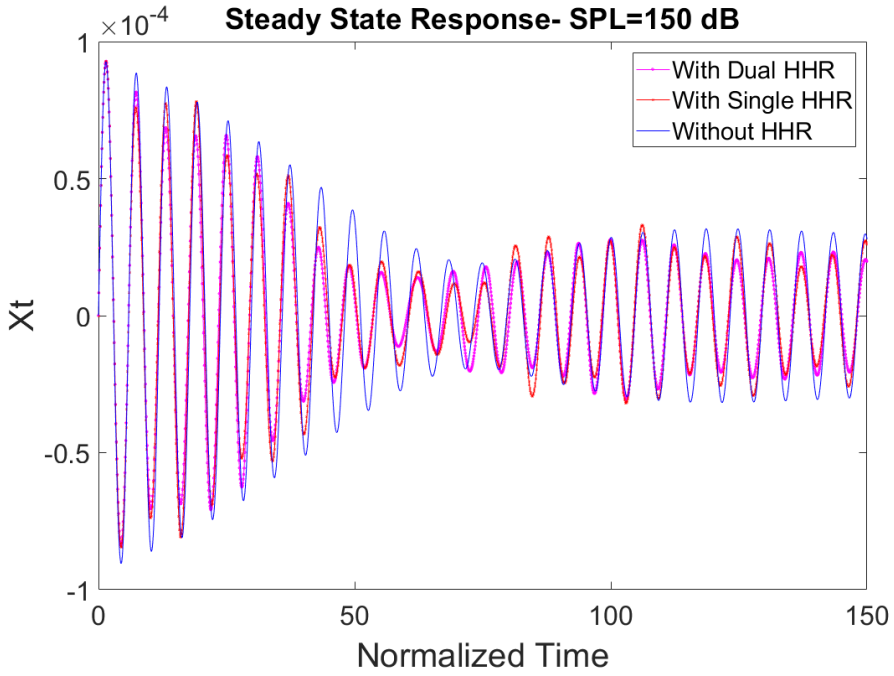

Figure 4.18: Steady State Response for Dual HHR Coupled with Kundt Tube

From figure 4.18 we can see that the absorption of the energy is better for the case with the coupled dual HHR as the displacement in the middle of the Kundt tube is the smallest. In fact, coupling a dual HHR allows for absorbtion of energy in a faster manner, compared to the system with a single HHR.

B) Transient Response

In order to simulate the free vibrations regime, a sinusoidal signal to the small tube with the frequency 450 Hz is sent to excite the acoustical mode in the stationary regime. Then the signal is stopped and the decreasing evolution of the response is recorded, for three configurations: the tube with a dual HHR, with a single HHR and without coupled HHRs, and for levels of incident amplitude 150 dB.

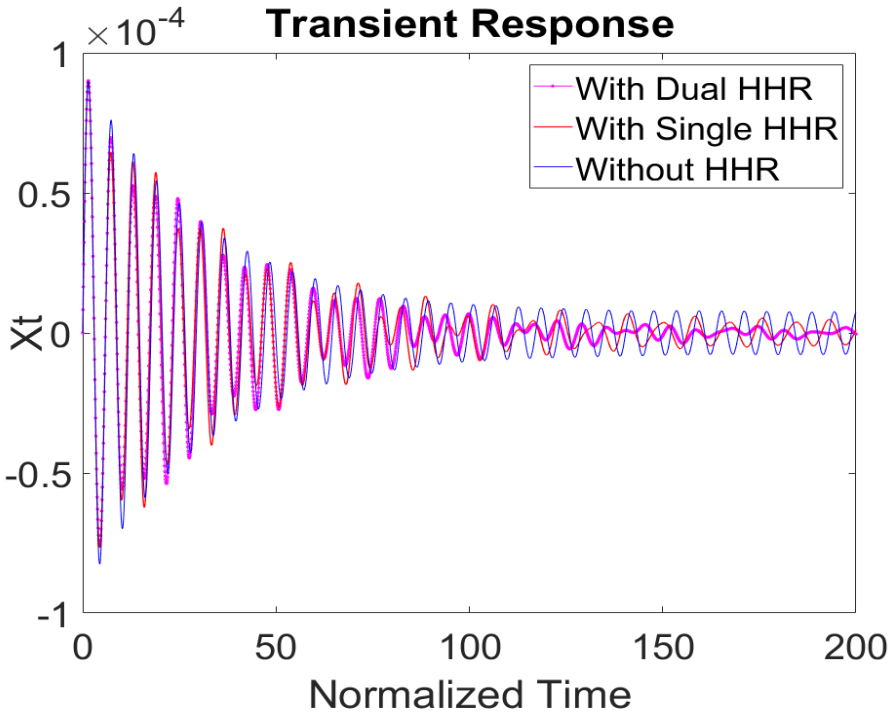

Figure 4.19: Frequency History for Dual HHR Coupled with Kundt Tube

Similar to the result obtained in the steady state solution, figure 4.19 shows that the absorption of the energy is better for the case with the coupled HHR as the displacement in the middle of the Kundt tube is the smallest.

C) Frequency History

In order to simulate the stationary response, a sweep sinusoidal signal is sent to study the behavior of the system as a function of frequency. The results are shown in Figure 4.20.

In Figure 4.20, similar to the one single peak that appears in the single HHR system described in section 4.4, the curve representing coupling a dual nonlinear resonator stays below the curve with a single HHR. Consequently, the dual nonlinear HHR is efficient, not only for a single frequency, but also for a larger band of frequencies. A phase shift in the resonance frequency is produced because of the coupled HHRs.

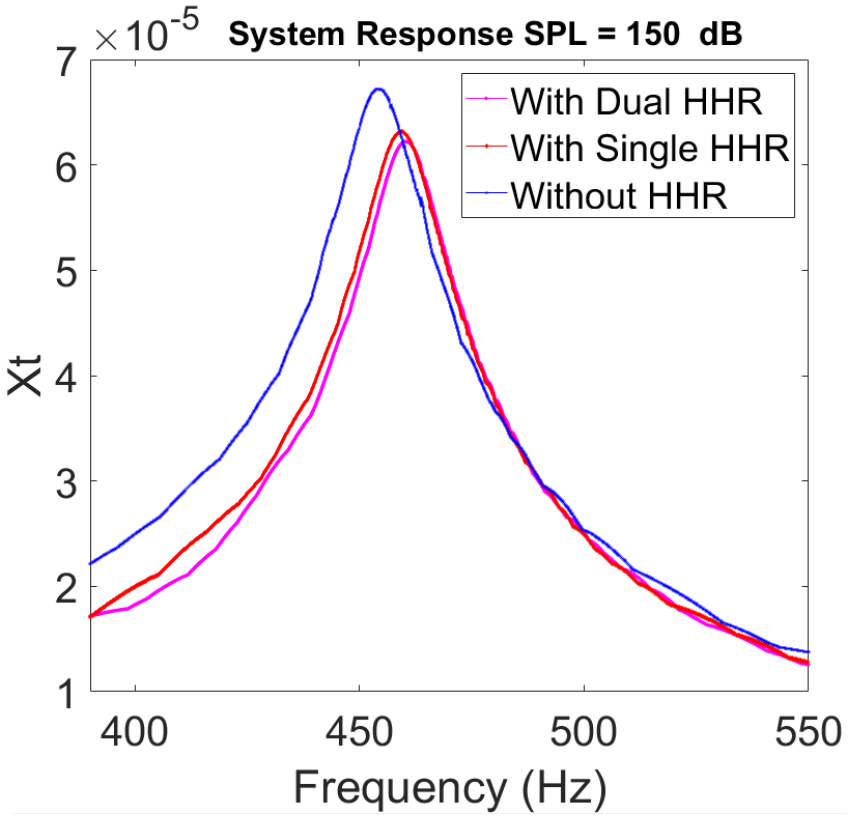

Figure 4.20: Frequency History for Dual HHR Coupled with Kundt Tube

D) Time Hisotry

A periodic response is illustrated from the time history shown in figure 4.21. Pressure amplitude at the middle of the Kundt tube is the smallest in the case of the coupld dual HHR, which is consistent with the preceding results.

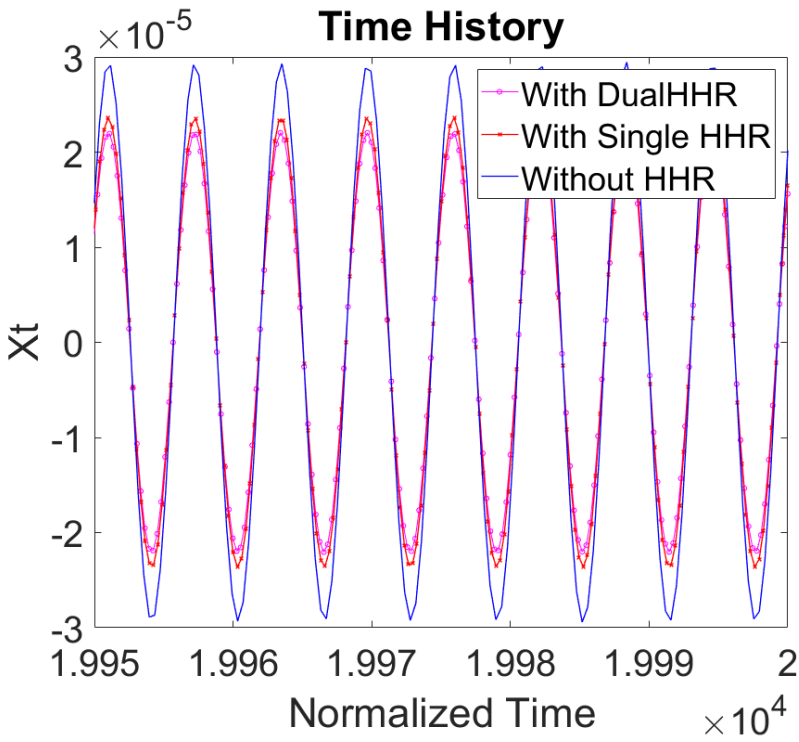

Figure 4.21: Time History for Dual HHR Coupled with Kundt Tube

CHAPTER 5

CONCLUSIONS AND RECOMMENDATIONS

In this thesis an analysis was made to examine the performance of Helmholtz resonators under different configurations using linear and nonlinear mathematical models. The resonators under investigation were considered to be attached to acoustic duct in one scenario and as a component of Kundt tube and coupling box resonator system. Helmholtz resonators were idealized as lumped parameter vibrating systems. The mass, damping and stiffness matrices were established and used to solve the equations of motion. Mathematical codes were developed for the acoustic analysis of these Helmholtz resonators. The mechanical structures that resembling the HHRs were analyzed in the time and frequency domains for specific incident waves.

Two types of Helmholtz resonators were considered, resonators with a single neck and a single volume (single HHR) and resonators with two necks and two volumes (dual HHR). Both types of resonators were analyzed as linear systems and then as nonlinear systems. Under linear analysis, resonant frequencies of the resonators and their effectiveness on the duct transmission loss were studied for single and dual HHRs. For the single HHR, one resonant frequency exists, while for dual HHRs, two resonant frequencies exist. When the area ratio of the two necks is increased, it is observed that the ratio of resonant frequencies is increased.

Under the nonlinear analysis, phase portraits, bifurcation diagram, time history and frequency analysis were conducted for the single and the dual Helmholtz resonators. These

results were compared to their counterpart obtained results for the linear analysis. It is observed that, the nonlinear HHRs showed a softening behavior at low sound pressure levels and hardening behavior at high sound pressure levels. The obtained results from nonlinear analysis explain the appearance of excess average pressure inside the resonator and a net reaction force acting on the resonator itself.

As for the second scenario of analyzing the HHR connected to a coupling box and Kundt tube in series. It was shown that transferring energy from one acoustical mode to the Helmholtz resonator is possible. It was also shown that the attenuation of acoustic energy is enhanced in the case of coupled dual HHRs over the coupled single HHR.

Future work built on this study can include the optimization techniques for designing improved applications of multi-Helmholtz resonator system under nonlinear analysis. Also, analyzing the effect of changing the fluid's properties on the performance of the Helmholtz resonator.

REFERENCES

[1] Science Daily, Acoustics. https://www.sciencedaily.com/terms/acoustics.htm. (accessed 15 November 2017).

[2] Education, Sound Physics: The difference between Sound and Noise. https://www.education.com/science-fair/article/ear-noise-physics-society/. (accessed 20 November 2017).

[3] Teresa Bravo , C. Maury, Sound attenuation and absorption by micro-perforated panels backed by anisotropic fibrous materials. Theoretical and experimental study. 2018, Journal of Sound and Vibration 425:189-207 · July.

[4] Noise Control Engineering, Acoustic Attenuators, https:// noisecontrolengineering.com.au/acoustic-attenuators/. (accessed 20 January 2018).

[5] Bob Peters, Acoustics and Noise Control, third edition, Harlow, Essex, England; New York: Pearson Education, 1982.

[6] The Engineering Toolbox, Classification of Noise Reduction Silencers, https://www.engineeringtoolbox.com/noise-reduction-silencers-d_81.html (accessed 12 February 2018).

[7] Chenzhi CAI, Cheuk MAK, Classical Noise attenuation capacity of a Helmholtz resonator. 2018, 116 (2018) 60–66.

[8] Cai C, Mak CM, Wang X., Noise attenuation performance improvement by adding Helmholtz resonators on the periodic ducted Helmholtz resonator system. 2017, Applied Acoustic 122:8-15.

[9] Mak CM, Yang J., A prediction method for aerodynamic sound produced by closely space element in air ducts.2000, J Sound Vibration ;229(3):743 –53.

[10] Guancong Ma, Ping Sheng, Acoustic metamaterials: from local resonances to broad horizons.2016, Science Advance; Vol. 2, no. 2, e1501595.

[11] Rayleigh JWS., The theory of sound. 2nd revised and enlarged ed., New York: Dover, 1945.

[12] Selamet A, Lee I-J., Helmholtz resonator with an extended neck.2003, J Acoustic Soc Am 2003; 113:1975–85.

[13] Munjal ML., Acoustics of ducts and mufflers with application to exhaust and ventilation system design. 2014, New York: Wiley.

[14] M.B. Xu, A. Selamet, H. Kim, Dual Helmholtz resonator.2010, Applied Acoustics 71-822–829.

[15] Munjal ML., Acoustics of ducts and mufflers, second edition, New York: Wiley,1987.

[16] Forner, K., Askin Temiz, M., Polifke, W., Lopez Arteaga, I., On the nonlinear influence of the edge geometry on vortex shedding in the Helmholtz resonators.2015, The 22nd International Congress on Sound and Vibration, 12-16 July 2015, Florence, Italy.

[17] Kumar Singh, Rienstra, S.W., A Systematics impedance model for nonlinear Helmholtz resonator liner. 2013, 19th AIAA/CEAS Aeroacoustics Conference, 27-29 May, Berlin, Germany.

[18] Yu, G.K., Zhang, Y.D., Shen, Y., Inducing passive nonlinear energy sinks in vibrating systems.2001, Journal of Vibration and Acoustics.

[19] Music Acoustics, Helmholtz Resonance, https://newt.phys.unsw.edu.au/jw/Helmholtz.html. (accessed on 21 March 2018).

[20] W Wang, Y Zhang, Q Zhou, X Peng, J Feng, and X Jia, Pulsation damping of the reciprocating compressor with Helmholtz resonator. 2017, IOP Conf. Series: Materials Science and Engineering 232- 012013

[21] Boom Speaker, Noise Level Chart (Decibel Chart), https://boomspeaker.com/noise-level-chart-db-level-chart (accessed on 21 March 2018).

[22] PHYSCLIPS, What is a Decibel, http://www.animations.physics.unsw.edu.au/jw/dB.htm, (accessed 11 January 2018) .

[23] Hyper physics, Sensitivity of Human Ear, http://hyperphysics.phy-astr.gsu.edu/hbase/Sound/earsens.html (accessed on 15 April 2018).

[24] Mamoon Hroob, Acoustic noise control using multiple expansion chambers. 2011, Thesis, King Fahd University of Petroleum and Minerals.

[25] Grab Cad Community, Reflective or Reactive Silencer, https://grabcad.com/library/reflective-or-reactive-silencer-1 (accessed on 17 April 2018).

[26] Risonatori di Helmholtz, https://sites.google.com/site/aureligliologallitto/collezionestorica/catalogo/acustica/resonatori di Helmholtz, (accessed 27 April 2018).

[27] Bell L. and Bell D., Industrial noise control, second edition revised and expanded Dekker Inc. New York, 1975.

[28] Hanbo Jiang1, Alex Siu Hong Lau1, Xun Huang1,2, Sound wave scattering in a flow duct with azimuthally non-uniform liners. Fluid Mech. (2018), vol. 839, pp. 644–662.

[29] Deming Wan, Dirk Tomas Soedel, Two degree of freedom Helmholtz resonator analysis. Noise and Vibration 2004 (SP-1867)

[30] Rogério Cora, Cristiane Aparecida Martins ⇑, Pedro Teixeira Lacava, Acoustic instabilities control using Helmholtz resonators. Applied Acoustics 77 (2014) 1–10

[31] Richoux, O., Tournat, V., Le Van Suu, T., Comportement nonlinéaire des bands interdites dans un réseau acoustiqueunidimensionnel. Congrès Français d'Acoustique (2006).

[32] Kundt, August, Acoustic experiments. The London, Edinburgh, and Dublin Philosophical Magazine and Journal of Science. Vol. 35 no. 4. UK: Taylor & Francis. pp. 41–48. Retrieved 2009-06-25.

[33] Mohammad Elmalki, Ali Khettabi, An analytical study by transfer matrix and Green's method of a periodic lattice formed by dual Helmholtz resonators (DHR). 3rd International Conference on Electrical and Information Technologies ICEIT’2017

[34] Selamet A, Xu MB, Lee I-J, Huff NT, Helmholtz resonator lined with absorbing material. J Acoustic Soc Am 2005;117:725–33.

[35] Chenzhi Cai, Cheuk Ming Mak, Acoustic performance of different Helmholtz resonator array configurations. Applied Acoustics 130 (2018) 204-209.

[36] Griffin S, Lane SA, Huybrechts S., Coupled Helmholtz resonators for acoustic attenuation. J Vib Acoust 2001;123:11–7.

[37] Muhammad A. Hawwa, Multiple Helmholtz Resonators, US Patent Number 8,418,804 B1, Apr. 16, 2013.

[38] V. Alamo Vargas · E. Gourdon, A. Ture Savadkoohi. Nonlinear softening and hardening behavior in Helmholtz resonators for nonlinear regimes, Springer Science+Business Media B.V. 2017.

[39] Frahm, H., Device for damping vibrations of bodies. US Patent 989,958 (1911).

[40] Alireza Ture Savadkoohi·Bastien Vaurigaud· Claude-Henri Lamarque·Stéphane Pernot. Targeted energy transfer with parallel nonlinear energy sinks, part II: theory and experiments, Springer Science+Business Media B.V. 2011.

[41] L. I. Manevitch, E. L. Manevitch, and C.-H. Lamarque, Toward the design of an optimal energetic sink in a strongly inhomogeneous two-degree-of-freedom system. Journal of Applied Mechanics, vol. 74, pp. 1078–1085, 2007.

[42] L. I. Manevitch, New approach to beating phenomenon in coupled nonlinear oscillatory chains. Archive of Applied Mechanics, vol. 77, no. 5, pp. 301–312, 2007.

[43] C. Bréard, A. Sayma, M. Imregun, A. G. Wilson, and B. J. Tester, A CFD-based nonlinear model for the prediction of tone noise in lined ducts. 7th AIAA/CEAS Aeroacoustics Conference, 2001, AIAA-2001-2176.

[44] C. K. W. Tam and K. A. Kurbatskii, Microfluid Dynamics and Acoustics of Resonant Liners. AIAA Journal, Vol. 38, No. 8, 2000, pp. 1331–1339.

[45] Q. Zhang, D. J. Bodony, Numerical simulation of two-dimensional acoustic liners with high-speed grazing flow. AIAA Journal, Vol. 49, No. 2, pp. 365–382.

[46] D. Innes and D. G. Crighton, On a nonlinear differential equation modelling Helmholtz resonator response. Journal of Sound and Vibration, Vol. 131, No. 2, 1989, pp. 323–330.

[47] L.Q. Chen, C.J. Cheng, N.H. Zhang,Chaotic motion of viscoelastic beams with geometric and physical nonlinearities. Eng. Mech. 18 (1) (2001) 1–6.

[48] Guanrong Ghen, An overview of bifurcation, chaos and nonlinear dynamics in control systems. Departamento de Ing. Electrica, Universidad Nacional de1 Sur, Avda. Alem 1253, (8000) Bahia Blanca, Argentina

[49] Cochelin, B., Herzog, P., and Mattei, P.-O., 2006, "Experimental evidence of energy pumping in acoustics," C. R. Mec., 334(11), pp. 639–644

[50] Bonet, J., Martínez-Giménez, F. Peris, A. A Banach space which admits no chaotic operator. Bulletin of the London Mathematical Society. 33 (2): 196–8-2001.

[51] Ricardo R. Boullosa and Felipe Orduna-Bustamante, The reaction force on a Helmholtz resonator driven at a high sound pressure amplitudes, Centra de Instrumentos, Universidad Nacional Autonoma de Mexico March 1992.

[52] Gourdon, E., and Ture Savadkoohi, A., Nonlinear structuring of Helmholtz resonators for increasing the range of sound absorption. The 10th European Congress and Exposition on Noise Control Engineering (Euro Noise), Maastricht, The Netherlands, May 31–June 3, pp. 973–976-2015.

[53] Sivian, L. J., Acoustic impedance of small orifices. J. Acoust. Soc. Am., 7(2), pp. 94–101, 1935.

[54] Bolt, R. H., Labate, S., and Ingard, U, The Acoustic reactance of small circular orifices. J. Acoust. Soc. Am., 21(2), pp. 94–97-1949.

[55] Ingard, U., and Ising, H., Acoustic nonlinearity of an orifice. J. Acoust. Soc. Am., 42(1), p. 6-1967.

[56] Achilleos, V., Richoux, O., Theocharis, G., and Frantzeskakis, D. J., Acoustic solitons in waveguides with Helmholtz resonators: transmission line approach. Phys. Rev. E - Stat., Nonlinear, Soft Matter Phys., 91(2), p. 023204, 2015.

VITA

Name: MAHER OMAR AL TURK

Place of Birth: Ibn Al Shater Street, Al-Bayader, Amman, PO Box #11185,Jordan.

Nationality: Jordanian

Permanent Address: Al Raka,

Khobar, Saudi Arabia.

Telephone: +962799108584

Email Address: maher.alturk@gmail.com

Educational Qualification:

MSc (Mechanical Engineering)

Dec 2018

King Fahd University of Petroleum and Minerals

Dhahran, Saudi Arabia.

B. Tech. (Mechanical Engineering)

June 2014

University of Jordan.

- Publications for this research work are under review, they will be released by one of the international journals on the soonest.